TABLE 2. Effect of the P101L mutation on the generation and transmission of infectious prions

Inoculum[a,b]	Recipients[b]	PrP^C expression level[c]	Time to disease (days ± SEM)	n/n_0[d]
None	Tg(MoPrP,P101L)196	1	552 ± 34	9/32
None	Tg(MoPrP,P101L)2866	8	132 ± 2	19/19
Tg(MoPrP,P101L)2866	CD-1	1	>700	0/8
Tg(MoPrP,P101L)2866	Tg(MoPrP-A)4053	8	>700	0/7
Tg(MoPrP,P101L)2866	Tg(MoPrP,P101L)196	1	305 ± 17	10/10
Tg(MoPrP,P101L)2866	Tg(MoPrP,P101L)196	1	263 ± 12	8/8
Tg196(2866)	Tg(MoPrP,P101L)196	1	351 ± 13	8/8
Non-β-MoPrP(89-143,P101L)[e]	Tg(MoPrP,P101L)196	1	632	1/8
β-MoPrP(89-143,P101L)[e,f]	Tg(MoPrP,P101L)196	1	360 ± 30	20/20
Tg196(β-MoPrP(89-143,P101L))[g]	Tg(MoPrP,P101L)196	1	349 ± 8	8/8
Tg196(β-MoPrP(89-143,P101L))[g]	Tg(MoPrP,P101L)196	1	351 ± 9	9/9
Tg196(β-MoPrP(89-143,P101L))[g]	Tg(MoPrP,P101L)196	1	327 ± 9	8/8
CD-1(RML)	CD-1	1	131 ± 0	29/29
CD-1(RML)[f]	Tg(MoPrP,P101L)196	1	229 ± 6	6/6
Tg196(RML)[g]	Tg(MoPrP,P101L)196	1	175 ± 1	7/7
Tg196(RML)[g]	Tg(MoPrP,P101L)196	1	186 ± 3	9/9
C57(139A)	CD-1	1	144 ± 2	14/14
C57(139A)[f]	Tg(MoPrP,P101L)196	1	425 ± 4	9/9
Tg196(139A)[g]	Tg(MoPrP,P101L)196	1	179 ± 8	9/9
Tg196(139A)[g]	Tg(MoPrP,P101L)196	1	198 ± 6	9/9
CD-1(301V)	CD-1	1	230 ± 3	10/10
CD-1(301V)	B6.I	1	132 ± 1	10/10
B6.I(301V)	B6.I	1	116 ± 1	17/17
B6.I(301V)	CD-1	1	224 ± 5	8/8
B6.I(301V)[f]	Tg(MoPrP,P101L)196	1	113 ± 4	9/9
B6.I(301V)[f]	Tg(MoPrP,P101L)196	1	127 ± 2	3/3
Tg196(301V)[g]	Tg(MoPrP,P101L)196	1	130 ± 3	5/5
Tg196(301V)[g]	Tg(MoPrP,P101L)196	1	129 ± 1	4/4

[a] Original prion inocula (RML, 139A, 301V) were obtained from *Prnp*[a] (C57, CD-1) and/or *Prnp*[b] mice (B6.I) or from spontaneously ill Tg(MoPrP,P101L)2866 mice. Homogenates used for transmissions originated from spontaneously ill or prion-inoculated mice at time of disease onset. The prion strain is shown in parentheses and the text preceding the parenthesis indicate the host in which it was last propagated.

[b] All Tg(MoPrP,P101L) mice were $Prnp^{0/0}$.

[c] Levels of PrP^C expression are compared with that of adult, wt FVB mice.

[d] Number of ill mice (n) over the total number of mice under observation (n_0).

[e] Data from reference 29.

[f] These inoculations correspond to the primary transmissions.

[g] Inocula used for these secondary transmissions were prepared from brains obtained in the primary transmissions from spontaneously ill or prion-inoculated mice at time of disease onset.

MoPrP(89-143,P101L) peptide. Four rabbits preselected for the low reactivity of their sera against homogenates from wt mouse brains were immunized subcutaneously with 1 ml of the MoPrP(89-143,P101L) peptide (250 μg/ml in PBS-RIBI adjuvant). This procedure was performed three times at 3-week intervals. Rabbits were bled 14 days after the final immunization procedure, and their sera were tested by Western blotting for reactivity against MoPrP(P101L). The serum from rabbit 5449 displayed strong reactivity against MoPrP(P101L), MHu2M(P102L), and HuPrP(P102L) but not against wt controls (Fig. 1). The epitope mapping with overlapping synthetic peptides demonstrated two dominant epitopes: one between residues 94 and 108 and a second between residues 129 and 143 (data not shown). Western blot analyses were performed as previously described (4), using anti-PrP 3F4 monoclonal antibody at a 1:2,500 dilution (30), RO73 polyclonal antiserum at a 1:5,000 dilution (43), or 5449 polyclonal antiserum at a 1:1,000 dilution. Blots were developed using the enhanced chemiluminescence system (Amersham Life Science, Arlington Heights, Ill.).

Detection of PrP^{Sc} by the CDI. Samples were processed for the CDI using time-resolved fluorescence spectroscopy, as previously described (39). Samples were split into two aliquots, one of which was kept untreated (native) while the second (denatured) was treated with one volume of 8 M guanidinium hydrochloride and heated at 80°C for 5 min. Both aliquots were further diluted 20-fold with a water-PI mixture. Samples were loaded in triplicates on 96-well polystyrene microplates (OptiPlate HTRF-96; Perkin-Elmer, Boston, Mass.) that were either precoated with the R1 recombinant fragment antibody (35) or preactivated with gluteraldehyde (0.2% in PBS [pH 7.4]; 2 h). The plates were incubated for 2 h at room temperature and blocked overnight with Tris-buffered saline (20 mM Tris-HCl [pH 7.5], 1% bovine serum albumen, 6% sorbitol) at 4°C. Primary antibodies were then added to the plates. The anti-PrP RO73 polyclonal antiserum was used at a 1:1,000 dilution with R1-coated plates, and the 5449 polyclonal antiserum was used at a 1:1,000 dilution on gluteraldehyde-activated plates, for 2 h at 37°C. Plates were washed three times with TBS–0.05% Tween 20 and incubated for 1 h with a Europium (Eu)-labeled, anti-rabbit antibody (Delfia, no. AD0105; 1:5,000). Plates were washed seven times with a Eu enhancement solution (Wallac, Turku, Finland) and read using a Discovery fluorescence detector (Perkin-Elmer). The difference in binding between the native (N) and denatured (D) states is expressed as the D:N ratio. A mathematical model was developed to calculate the β-sheet content in PrP using these values (39). The concentration of PrP in the samples was calculated from calibration curves generated with the β-rich recombinant MoPrP(89-231) for RO73 or with synthetic MoPrP(89-143,P101L) for 5449. The signal obtained from normal Tg(MoPrP,P101L)196/$Prnp^{0/0}$ was used as an internal reference between plates.

Histopathological procedures. Brains were removed from euthanized animals shortly after death and were frozen on dry ice or immersion fixed in 10% buffered formalin for inclusion in paraffin. Histoblots were performed on 10-μm, frozen coronal sections, transferred to a nitrocellulose membrane, and processed for immunohistochemistry using anti-PrP RO73 polyclonal antiserum, as previously described (45). Eight-micrometer paraffin sections were stained with hematoxylin and eosin for evaluation of neurodegenerative changes. Evaluation of reactive astrocytic gliosis was performed by immunostaining of glial fibrillary

TABLE 3. Propagation of GSS(P101L) prions in transgenic mice

Inoculum[a]	Treatment	Time to disease (days ± SEM)	n/n_0[b]	Time elapsed (days)
Tg196[c]	None	478 ± 37	6/7	>500
	PTA	432	1/8	>550
	PK/PTA	468 ± 22	2/9	>500
	PTA/PK	483	1/9	>500
Tg2866[d]	None	305 ± 17	10/10	
	PTA	278 ± 16	10/10	
	PK/PTA	262 ± 12	8/8	
	PTA/PK	226 ± 8	10/10	
Tg196(2866)[e]	None	351 ± 13	8/8	
	PTA	294 ± 4	9/9	
	PK/PTA	286 ± 3	10/10	
	PTA/PK	279 ± 7	9/9	
Tg196(196(301V))[f]	None	144 ± 4	6/7	>550
	PTA	148 ± 6	7/7	
	PK/PTA	126 ± 3	5/5	
	PTA/PK	131 ± 3	8/8	

[a] All transmissions were carried out using Tg(MoPrP,P101L)196/*Prnp*$^{0/0}$ mice as recipients. For each inoculum series, a pool of at least three brain homogenates was split among the following treatments: none, untreated; PTA, sodium phosphotungstate precipitation; PK/PTA, PK digestion followed by PTA precipitation; PTA/PK, PTA precipitation followed by PK digestion.

[b] Number of ill animals (n) over number of animals under observation (n_0).

[c] Samples from clinically normal Tg(MoPrP,P101L)196/*Prnp*$^{0/0}$ mice age-matched with ill Tg196(2866) mice at ~300 days of age.

[d] Tg2866 corresponds to spontaneously ill Tg(MoPrP,P101L)2866/*Prnp*$^{0/0}$ mice at ~130 days of age.

[e] Tg196(2866) corresponds to ill Tg(MoPrP,P101L)196/*Prnp*$^{0/0}$ mice (~300 days of age) following inoculation with brain homogenates from spontaneously ill Tg2866 mice.

[f] Tg196(196(301V)) inoculum was obtained from the secondary transmission of 301V prions into Tg(MoPrP,P101L)196/*Prnp*$^{0/0}$ mice (see Table 1).

acidic protein using a rabbit antiserum (Dako, Carpinteria, Calif.), as previously described (34). Hydrolytic autoclaving immunodetections were carried out on paraffin-embedded sections (34).

RESULTS

Serial passage of peptide-induced GSS in Tg196 mice. In earlier studies, we reported that the i.c. inoculation of a 55-mer peptide, designated MoPrP(89-143,P101L), carrying the P101L mutation and folded into β-rich conformation, induces central nervous system (CNS) degeneration in Tg196 mice (Table 2) (29). All of the Tg196 mice succumbed to disease at ~360 days after inoculation with this peptide. Approximately 30% of uninoculated Tg196 mice developed disease at ~550 days of age.

Brain homogenates from three Tg196 mice that developed disease after peptide inoculation were inoculated into three separate groups of Tg196 mice. All of the mice developed disease, with similar mean incubation periods of 327 days, 349 days, and 351 days (Table 2). These results argue convincingly that the β-rich MoPrP(89-143,P101L) peptide induces the accumulation of infectious prions that can be serially propagated in Tg196 mice. We conclude from these findings that the β-rich 55-mer peptide either initiated the formation of de novo GSS prions in the host or is itself a synthetic prion.

Overexpression of MoPrP(P101L) induces spontaneous neurodegeneration. When high levels of MoPrP(P101L) were expressed in the brains of Tg2866 mice, mice developed spontaneous neurodegeneration at ~130 days of age. Extracts prepared from the brains of two ill Tg2866 mice inoculated into two groups of Tg196 mice caused disease in 263 days and 305 days.

Neuropathology of Tg196 mice. Often, prion strains can be distinguished by the histopathological distribution of lesions, the pattern of PrP^{Sc} accumulation, and the presence and type of amyloid plaques produced in infected brains (20) (Fig. 2). Tg196 mice inoculated with brain extracts prepared from spontaneously ill Tg2866 mice showed neuropathologic changes similar to those of Tg196 mice inoculated with the MoPrP (89-143,P101L) peptide (Fig. 2B and C). Tg196 mice that developed disease after inoculation with the MoPrP(89-143,

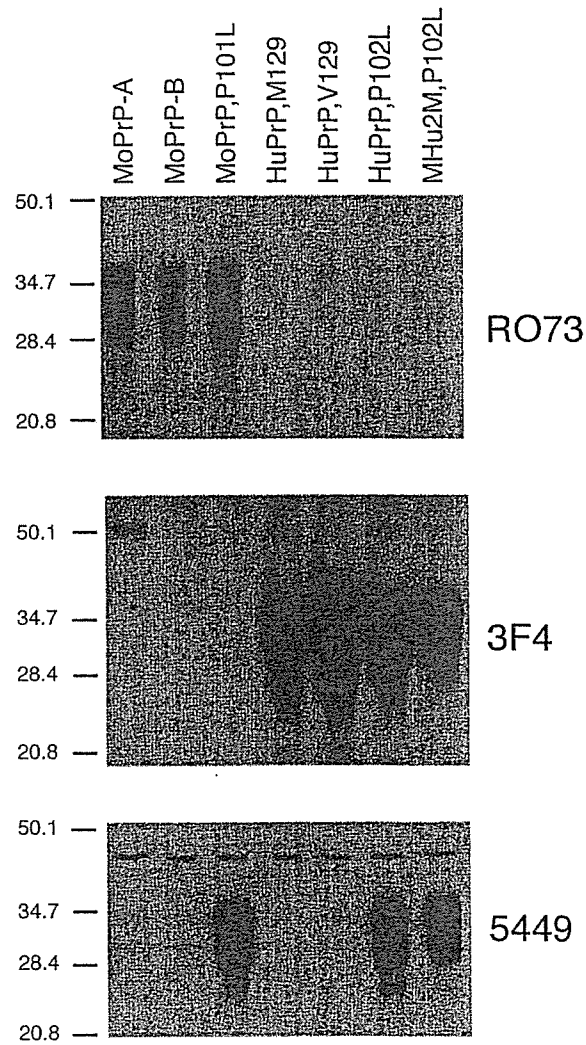

FIG. 1. Selective immunoreactivity of rabbit polyclonal antiserum 5449 raised against the MoPrP(89-143,P101L) peptide with PrPs carrying the P101L mutation. Brain homogenates (20 μg of total protein per lane) from mice expressing wt MoPrP-A (FVB), wt MoPrP-B (ILn/J), MoPrP(P101L) [Tg(MoPrP,P101L)196/*Prnp*$^{0/0}$], HuPrP(M129) [Tg(HuPrP,M129)440/*Prnp*$^{0/0}$], HuPrP(V129) [Tg(HuPrP,V129)152/*Prnp*$^{0/0}$], HuPrP(P102L) [Tg(HuPrP,P102L)7/*Prnp*$^{0/0}$], and MHu2M(P102L) [Tg(MHu2M,P102L)69/*Prnp*$^{0/0}$] were processed. Western blots were developed using the anti-PrP(P101L) 5449 polyclonal antiserum, and for comparison, with the anti-PrP RO73 polyclonal antiserum and the 3F4 monoclonal antibody. The apparent molecular weights of the migrated fragments are shown in thousands.

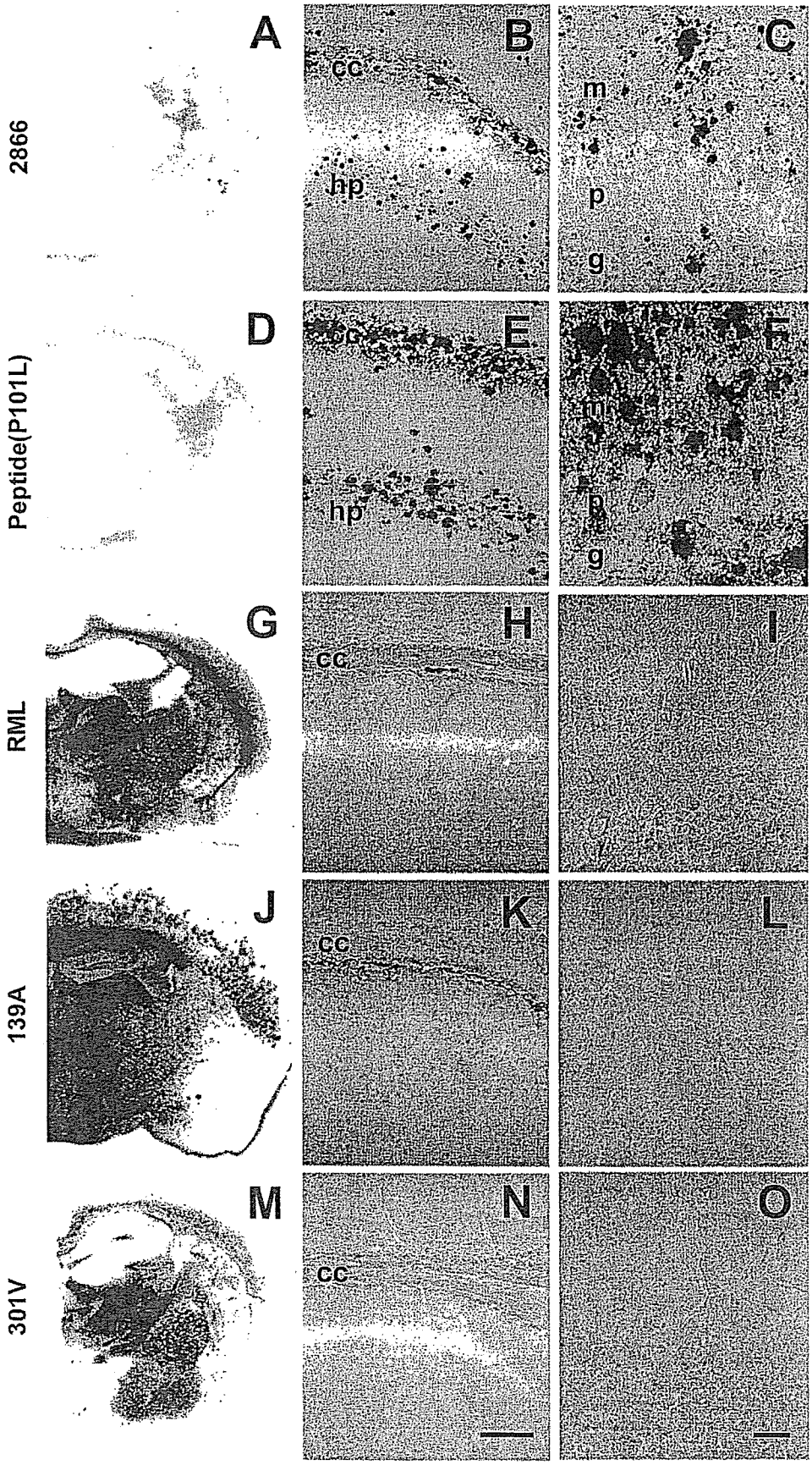
A
B
C
2866
cc
hp
m
p
g
D
E
F
Peptide(P101L)
cc
hp
m
p
g
G
H
I
RML
cc
J
K
L
139A
cc
M
N
O
301V
cc

P101L) peptide showed numerous large (70 μm), multicentric, GSS-like plaques in the neocortex, hippocampus, corpus callosum, caudate nucleus, globus pallidus, and cerebellar cortex (Fig. 2E and F). All of these plaques stained with anti-PrP antibodies. Severe spongiform changes and astrocytic gliosis associated with the loss of granule cells and numerous immature, GSS-like amyloid plaques were found in the cerebellum.

Prion strains from wt mice. Tg196 mice were susceptible to prion strains isolated in wt mice. RML and 139A strains were isolated from sheep with naturally occurring scrapie and passaged in $Prnp^{a/a}$ mice. In CD-1 ($Prnp^{a/a}$) mice, the incubation periods for RML and 139A prions were ~130 and ~145 days, respectively. When RML and 139A prions were inoculated into Tg196 mice, prolonged incubation periods of ~230 and ~425 days, respectively, were observed (Table 2); on second passage, the incubation times shortened to ~180 days and ~190 days, respectively. 301V prions were isolated from cattle with BSE by passage in $Prnp^{b/b}$ mice. When 301V prions were transmitted from $Prnp^{b/b}$ mice to Tg196 mice, incubation periods of ~120 days and ~115 days were observed on first and second passage, respectively. 301V prions have similar incubation periods in $Prnp^{b/b}$ and Tg196 mice but produce incubation periods of ~230 days in CD-1 mice.

These findings suggest that the P101L mutation creates a transmission barrier for propagation of the RML and 139A prion strains previously passaged in $Prnp^{a/a}$ mice. In contrast, the mutation poses no transmission barrier for 301V prions previously passaged in $Prnp^{b/b}$ mice. Taken together, our findings argue that the P101L mutation has an effect on incubation times similar to that of the L108F and T189V substitutions encoded in mouse $Prnp^{b}$ (49).

Intracerebral inoculation of Tg196 mice with the RML, 139A, and 301V prions resulted in neuropathological changes typical of experimental scrapie. The accumulation of $rPrP^{Sc}$ was evident using the histoblot method (Fig. 2G, J, and M) and vacuolation of the gray matter localized with sites of PrP^{Sc} accumulation (data not shown). Small (25 μm), subcallosal PrP plaques were also present in the brains of RML- and 139A-inoculated animals (Fig. 2H to I, K to L, and N to O). No plaques were found in the cerebella of mice inoculated with any of these three prion strains (Figs. 2I, L, and O).

Histoblotting revealed that each of the three prion strains produced a unique distribution of $rPrP^{Sc}$ in the gray and/or white matter (Fig. 2G, J, and M). For example, 139A prions produced intense PrP^{Sc} immunostaining in the hippocampus, but inoculation with RML and 301V prions did not produce PrP^{Sc} deposits in this region. Inoculation with RML prions resulted in a mild degree of vacuolation in layers IV through VI of the neocortex (data not shown) that correlated well with the medium-intensity immunostaining for PrP^{Sc} confined to the inner half of the neocortex (Fig. 2G). In animals inoculated with the 301V strain, immunostaining was not observed in the neocortex (Fig. 2M) and vacuolation was not detected (data not shown).

Biochemical detection of MoPrP(P101L) conformers. Earlier attempts using PK digestion for prolonged durations failed to identify altered forms of MoPrP(P101L) that feature in neurodegeneration. Therefore, we employed two new approaches. First, we took advantage of the ability of PTA to differentially precipitate PrP^{Sc} while leaving PrP^{C} in the supernatant fraction. Second, we employed alternative conditions for PK digestions by lowering the temperature to 4°C, a condition employed previously to demonstrate alterative forms that mutant PrPs can adopt (25). The protease resistance of MoPrP(P101L) conformers was probed using two different protocols: (i) digestion with 25 μg of PK/ml for 1 h at 37°C and (ii) digestion with 250 μg of PK/ml for 1 h at 4°C. In previous studies, we designated the latter protocol using digestion at 4°C as "mild PK" to distinguish it from the "harsh PK" protocol with digestion at 37°C (25). In the interest of clarity, here we designate digestion at 4°C as "cold PK" and simply refer to digestion at 37°C as "PK" (Table 1).

As previously described, $rPrP^{Sc}$(P101L) was undetectable in the brains of spontaneously ill Tg2886 or ill Tg196 mice after inoculation with mouse GSS(P101L) prions (27, 28, 47). Similar results were obtained with Tg196 mice inoculated with the β-rich MoPrP(89-143,P101L) peptide and in subsequent passages (Fig. 3F) (29). Low levels of $rPrP^{Sc}$(P101L) were detected in spontaneously ill Tg2866 mice only when samples were concentrated by ultracentrifugation (Fig. 3C). These low levels of $rPrP^{Sc}$(P101L) in brain homogenates from Tg mice infected with GSS(P101L) prions or the β-rich MoPrP(89-143,P101L) peptide contrast with the high levels of $rPrP^{Sc}$(P101L) in Tg196 mice inoculated with RML, 139A, or 301V prions (Fig. 3C and data not shown).

Traces of PTA-precipitable PrP were found in uninoculated, age-matched, control Tg196 and Tg(MoPrP-A)4053/$Prnp^{0/0}$ mice (Fig. 3B). In contrast, the PTA-precipitable PrP fraction was severalfold greater in the brains of spontaneously ill Tg2866 mice and in Tg196 mice inoculated with brain homogenates from spontaneously ill Tg2866 mice.

In the brains of spontaneously ill Tg2866 mice, high levels of a PrP^{Sc} fragment migrating to 22 to 24 kDa on Western blots was detected by cold PK digestion; PrP 22-24 is the cold PK-resistant fragment of $sPrP^{Sc}$(P101L) (Table 1). PrP 22-24 was also found in Tg196 mice following inoculation with mouse GSS(P101L) prions or with the β-rich MoPrP(89-143,P101L) peptide after first and second passages (Fig. 3D to F). The cold PK-resistant signal was stronger after PTA precipitation. Normal, age-matched Tg196 mice (~350 days of age) and Tg4053

FIG. 2. GSS-like neuropathological features in the absence of PK-resistant PrP^{Sc} in spontaneous and synthetic peptide-induced prion disease in Tg mice expressing the MoPrP(P101L) allele. The analyzed brains are from Tg(MoPrP,P101L)196/$Prnp^{0/0}$ mice inoculated with prions from spontaneously ill Tg(MoPrP,P101L)2866/$Prnp^{0/0}$ mice (A, B, and C), β-rich MoPrP(89–143,P101L) peptide (D, E, and F), or for comparison, with RML (G, H, and I), 139A (J, K, and L), or 301V (M, N, and O) prions. Distribution of $rPrP^{Sc}$ was determined by histoblotting (A, D, G, J, and M), and PrP-immunoreactive plaques were detected by hydrolytic autoclaving in the hippocampus (B, E, H, K, and N) and cerebellum (C, F, I, L, and O). Abbreviations: cc, corpus callosum; g, granule cell layer; hp, stratum radiatum of the CA1 region of the hippocampus; m, molecular layer; p, Purkinje cell layer. The bar in panel N represents 100 μm and applies to panels B, E, H, and K; The bar in panel O represents 30 μm and applies to panels C, F, I, and L.

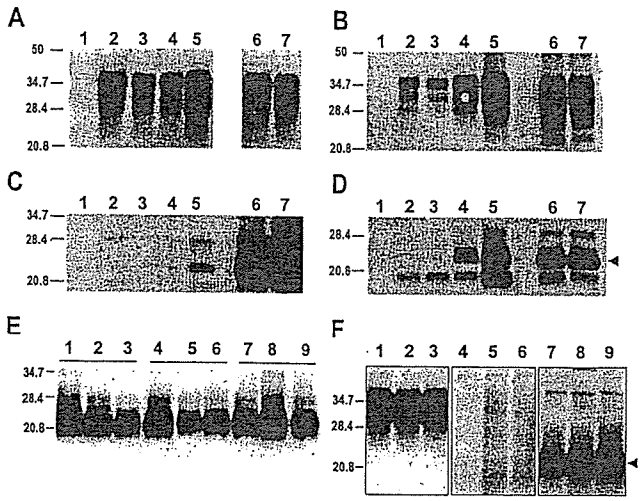

FIG. 3. Serial passage of aberrant PrP conformers in Tg(MoPrP, P101L) mice, detected by selective PTA precipitation and cold PK treatment. The 22- to 24-kDa PrP fragment (arrowheads) was found exclusively in Tg196 mice following inoculation with mouse GSS(P101L) prions or the β-rich MoPrP(89-143,P101L) peptide after both first and second passages. (A to D) Brain homogenates from uninoculated $Prnp^{0/0}$ mice (lane 1), Tg(MoPrP-A)4053/$Prnp^{0/0}$ mice (lane 2), uninoculated Tg(MoPrP,P101L)196/$Prnp^{0/0}$ mice (lane 3), Tg196 mice inoculated with brain homogenates from ill Tg2866 mice (lane 4), spontaneously ill Tg2866 mice (lane 5), Tg196 mice inoculated with RML prions (lane 6), or Tg196 mice inoculated with 301V prions (lane 7) are shown. Brain homogenates were untreated (A), precipitated with PTA (B), PK digested and subjected to ultracentrifugation (C), or subjected to cold PK digestion and precipitated with PTA (D). (E) Brain homogenates subjected to cold PK digestion and PTA precipitation from spontaneously ill Tg2866 mice (lanes 1 to 3), Tg196 mice inoculated with brain homogenates of diseased Tg2866 mice (lanes 4 to 6), or second passage of Tg2866 brain homogenates in Tg196 mice (lanes 7 to 9). (F) Brain homogenates from Tg196 mice inoculated with brain homogenates from ill Tg2866 mice (lanes 1, 4, and 7), β-rich MoPrP(89-134,P101L) peptide (lanes 2, 5, and 8), or second passage of MoPrP(89-134,P101L) peptide into Tg196 mice (lanes 3, 6, and 9). Samples were untreated (lanes 1 to 3), PK digested and ultracentrifuged (lanes 4 to 6), or subjected to cold PK digestion and PTA precipitation (lanes 7 to 9). Blots were developed using anti-PrP RO73 (A to D) or anti-PrP(P101L) 5449 polyclonal antisera raised against a random-coil MoPrP(89–143,P101L) peptide (E and F). The apparent molecular weights of the migrated fragments are shown in thousands.

mice (~140 days of age) did not display PrP 22-24 (Fig. 3D). A shorter PrP fragment of ~19 kDa was detected using the cold PK assay in all mice when blots were stained with anti-PrP RO73 polyclonal antiserum (Fig. 3D) but not when using the 5449 antiserum, which reacts only with residues 89 to 143 of MoPrP(P101L) (Fig. 3E and F). The 19-kDa fragment probably corresponds to the C-terminal portion of PrP.

Transmission of mouse GSS(P101L) prions. We measured prion infectivity in the brains of uninoculated Tg2866 mice after they spontaneously developed CNS dysfunction at ~130 days of age. Brain homogenates from Tg2866 mice were subjected to PTA precipitation alone or in combination with PK digestion before bioassay in Tg196 mice (Table 3). Untreated brain homogenates from Tg2866 mice produced disease in Tg196 mice at ~305 days, while PTA precipitation followed by PK digestion reduced the incubation time to ~225 days. This ~80-day reduction in the incubation time is highly significant, with a P value of <0.0014 (analysis of variance), arguing that the prions in the brains of Tg2866 mice are resistant to PK digestion.

Similar results were obtained when brain extracts were prepared from Tg196 mice previously inoculated with Tg2866 brain homogenates. The untreated homogenates from the Tg196(2866) mice produced disease in inoculated Tg196 mice after ~350 days, while PTA precipitation followed by PK digestion reduced the incubation time to ~280 days (Table 3). This ~70-day reduction in the incubation time is highly significant, with a P value of < 0.0005 (analysis of variance), arguing that the prions in the brains of Tg196(2866) mice are also resistant to PK digestion.

In contrast to the studies with inocula derived from the brains of Tg2866 mice, untreated inocula from the brains of neurologically normal Tg196 mice at ~300 days of age produced disease in six of seven Tg196 mice after ~480 days (Table 3). Moreover, inocula subjected to PTA precipitation followed by PK digestion produced disease at ~480 days but only in one of nine Tg196 mice. When 301V prions were inoculated into Tg196 mice, the incubation period was ~145 days, which was reduced by ~15 days when the inoculum was first subjected to PTA precipitation and PK digestion; this 10% reduction in incubation time is statistically insignificant. The 301V prions were initially isolated from BSE brain by passage in VM mice harboring the $Prnp^{b/b}$ alleles and subsequently passaged in B6.1 mice also carrying $Prnp^{b/b}$ alleles, with an incubation time of ~115 days (Table 2). On subsequent passages in Tg196 mice, the incubation times ranged from 115 to 145 days (Tables 2 and 3).

Age-dependent accumulation of prions in Tg2866 mice. We measured prion infectivity in the brains of Tg2866 mice by sacrificing the mice at various ages and inoculating their brain extracts into Tg196 mice. BH from Tg2866 mice sacrificed either at birth or at 56 days of age contained no detectable levels of prion infectivity, based on bioassays in Tg196 mice (Fig. 4E). Low levels of infectivity were found in 84-day-old Tg2866 mice: brain extracts from these mice inoculated into Tg196 mice induced disease in two of nine animals at ~440 days postinoculation (Fig. 4E). Brain extracts from 112-day-old Tg2866 mice produced disease after ~350 days of incubation in 9 of 10 animals. When Tg2866 mice developed signs of CNS dysfunction at ~130 days, the mice were sacrificed and their BH were inoculated into Tg196 mice. All eight inoculated Tg196 mice developed disease, with a mean incubation period of ~260 days (Fig. 4E). No infectivity was detected in the brains of age-matched, control Tg4053 mice (130 days of age), based on bioassays in Tg196 mice (0 of 10 animals, >500 days); Tg4053 mice express wt MoPrP at levels similar to mutant MoPrP(P101L) expressed in Tg2866 mice. This progressive shortening of incubation periods is consistent with an increase in the titer of infectious prions in the brains of Tg2866 mice as they age.

The progressive accumulation of infectious GSS(P101L) prions in Tg2866 mice as they aged correlated with the appearance of $sPrP^{Sc}$(P101L). PrP 22-24 was detected at 112 days and ~130 days using the cold PK digestion protocol (Fig. 4C). Curiously, Tg2866 mice showed a transient postnatal upregulation of mutant MoPrP(P101L) expression between 14 and 56 days of age (Fig. 4A). Levels of $sPrP^{Sc}$(P101L) were highest in

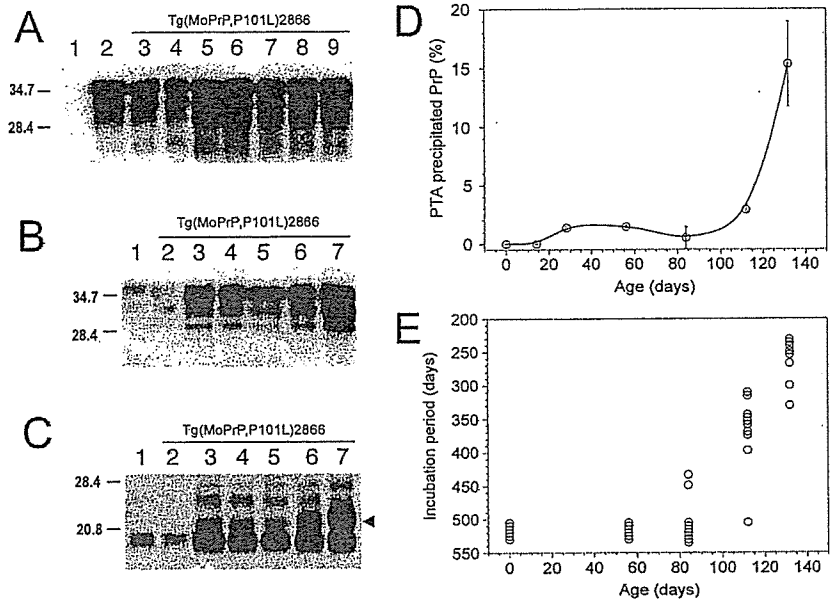

FIG. 4. Progressive accumulation of abnormal MoPrP(P101L) conformers (A to D) correlates with the accumulation of infectious prions (E) as a function of age in Tg(MoPrP,P101L)2866/$Prnp^{0/0}$ mice. Presymptomatic animals were sacrificed at birth, at 14 days, 28 days, 56 days, 84 days, or 112 days of age or at ~132 days (when diagnosed with CNS dysfunction). Blots were developed using the RO73 polyclonal antibody. The apparent molecular weights of the migrated fragments are shown in thousands. (A) Untreated brain homogenates from $Prnp^{0/0}$ mice (lane 1), Tg4053 mice (lane 2), or Tg2866 mice (lanes 3 to 9) sacrificed at birth (lane 3), 14 days (lane 4), 28 days (lane 5), 56 days (lane 6), 84 days (lane 7), 112 days (lane 8), or ~132 days (lane 9). (B) Brain homogenates from Tg4053 mice (lane 1), Tg2866 mice sacrificed at 14 days (lane 2), 28 days (lane 3), 56 days (lane 4), 84 days (lane 5), 112 days (lane 6), or ~132 days (lane 7). Samples were precipitated with PTA prior to immunoblotting. (C) Brain homogenates subjected to cold PK digestion followed by PTA precipitation. Lane assignments are as described for panel B. The presence of a 22-kDa to 24-kDa PrP fragment specific to infectious GSS prions is indicated by the arrowhead. (D) The accumulation of abnormal PrP conformers in the brains of aging Tg(MoPrP,P101L)2866/$Prnp^{0/0}$ mice was quantified using the CDI with the RO73 antiserum and a secondary Eu-labeled anti-rabbit polyclonal antibody. (E) The same brain homogenates from aging Tg(MoPrP,P101L)2866/$Prnp^{0/0}$ mice used in the CDI were inoculated into Tg(MoPrP,P101L)196/$Prnp^{0/0}$ mice to measure incubation times, which are inversely proportional to the prion titer (38). Animals that did not display signs of neurological dysfunction were sacrificed after 500 days.

Tg2866 mice at ~130 days of age, when these mice developed CNS disease (Fig. 4B).

GSS(P102L) prions in human patients and Tg mice. We assessed whether the progressive accumulation of abnormal PrP conformers observed in Tg2866 mice applies to GSS patients and to Tg mice expressing the MHu2M transgene with the corresponding P102L mutation, designated Tg(MHu2M,P102L)69/$Prnp^{0/0}$ mice. Tg69 mice developed CNS disease spontaneously at ~400 days of age; however, when Tg69 mice were inoculated with brain extracts from patients who died of GSS, they developed disease ~170 days after inoculation.

Brain samples from Tg69 mice and from patients with GSS were subjected to PTA precipitation alone or after cold PK digestion. These brain samples displayed increased levels of $sHuPrP^{Sc}$(P102L) compared to untreated samples (Fig. 5A, B, and D). Mutant HuPrP 22-24 was found in Tg69 mice at 200 days of age (Fig. 5D) and at much higher levels in spontaneously ill Tg69 mice at ~360 days of age (Fig. 5F and H).

Conformation-dependent immunoassay. The development of the CDI permitted measurement of both $rPrP^{Sc}$ and $sPrP^{Sc}$ (39). We used the CDI to measure the relative ratios of $rPrP^{Sc}$ and $sPrP^{Sc}$ in the brains of Tg196 and Tg2866 mice (Table 1). No $sPrP^{Sc}$(P101L) was detectable in the brains of uninoculated Tg196 mice, while $sPrP^{Sc}$(P101L) comprised ~15% of total PrP in spontaneously ill Tg2866 mice (Fig. 6A). As noted above, $sPrP^{Sc}$(P101L) is measured by cold PK digestion followed by PTA precipitation. In the brains of Tg196 mice inoculated with prions from Tg2866 mice, $sPrP^{Sc}$(P101L) accounted for ~20% of total PrP. In the brains of Tg196 mice inoculated with prions derived from sheep (RML) or cattle (301V), $sPrP^{Sc}$(P101L) comprised ~25% of total PrP. PK digestion followed by ultracentrifugation showed that $rPrP^{Sc}$ (P101L) was undetectable in the brains of uninoculated Tg196 mice. In contrast, $rPrP^{Sc}$(P101L) represented ~5% of the total PrP in the brains of spontaneously ill Tg2866 mice (Fig. 6A). In Tg196 mice inoculated with prions from Tg2866 mice, ~10% of total PrP was PK resistant; in Tg196 mice inoculated with either RML or 301V prions, ~20% of the total PrP was PK resistant.

When $rPrP^{Sc}$(P101L) was plotted as a function of the ratio of denatured (D) to native (N) PrP^{Sc}, as measured by time-resolved fluorescence spectrometry (Fig. 6B), the PrP^{Sc} (P101L) conformers found in the brains of spontaneously ill Tg2866 mice were distinct from those found in Tg196 mice inoculated with RML or 301V prions. The PrP^{Sc}(P101L) conformers found in spontaneously ill Tg2866 mice were indistinguishable from those found in the three groups of mice: (i) Tg196 mice inoculated with the MoPrP(89-143,P101L) peptide; (ii) Tg196 mice inoculated with brain extracts from ill Tg196 mice that were inoculated with the MoPrP(89-143, P101L) peptide; and (iii) Tg196 inoculated with brain extracts

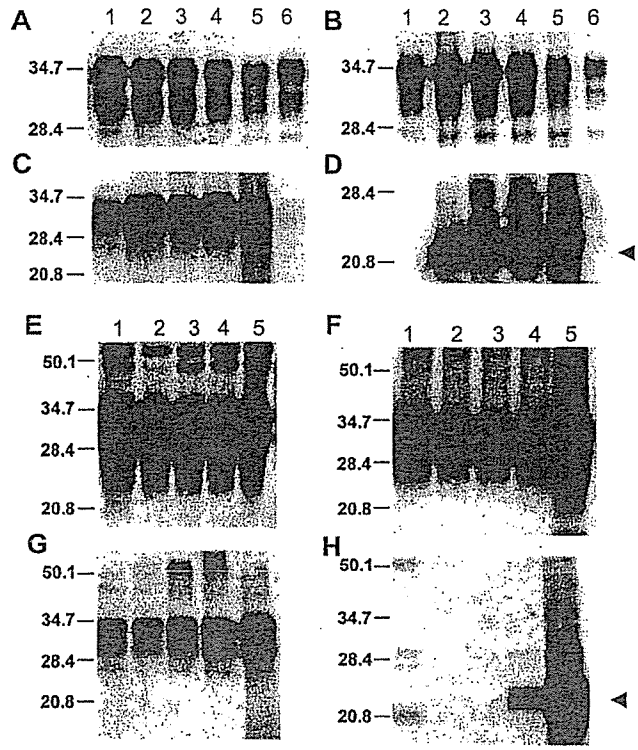

FIG. 5. Aberrant HuPrP(P102L) conformers present in the brains of GSS patients and GSS-inoculated Tg mice (A to D) are indistinguishable from those that progressively accumulate in spontaneously ill chimeric Tg(MHu2M,P102L) mice (E to H). Samples were developed using the 3F4 monoclonal antibody. The apparent molecular weights of migrated fragments are shown in thousands. The presence of a 22-kDa to 24-kDa PrP fragment specific to GSS prions is indicated by the arrowheads. (A to D) Brain homogenates from spontaneously ill Tg(MHu2M,P102L)69/*Prnp*$^{0/0}$ mice (lane 2), Tg(MHu2M,P102L) mice inoculated with homogenates from GSS patients expressing either Val (lane 3) or Met (lane 4) at codon 129, and a GSS(P102L,M129) patient (lane 5). As controls, homogenates from an age-matched, healthy Tg(MHu2M)*Prnp*$^{0/0}$ mouse (lane 1) and normal human brain (lane 6) are shown. (E to H) Brain homogenates from spontaneously ill Tg69 mice sacrificed at 50 days (lane 2), 100 days (lane 3), 200 days (lane 4), ~360 days (lane 5), when the mice became ill, demonstrate the accumulation of PrP^{Sc} conformers that are similar to those observed in GSS patients. As a control, homogenate from a healthy, age-matched Tg(MHu2M)*Prnp*$^{0/0}$ mouse (lane 1) is shown. Samples were untreated (A and E), precipitated with PTA (B and F), digested with PK followed by ultracentrifugation (C and G), or subjected to cold PK digestion followed by PTA precipitation (D and H).

from ill Tg2866 mice. These findings support the contention that the GSS prions either arising spontaneously in Tg2866 mice or induced in Tg196 mice by the 55-mer MoPrP(89-143, P101L) peptide are distinct from prion strains derived from sheep with scrapie (RML) and cattle with BSE (301V).

DISCUSSION

The results reported here permit, for the first time, biophysical correlations with prion infectivity generated in mice expressing MoPrP(P101L) transgenes. Although the first Tg mice expressing MoPrP(P101L) were constructed more than a decade ago (26, 27, 47), the lack of biophysically detectable alterations in mutant MoPrP(P101L) has compromised the utility of this model system, until now. Selective precipitation of PrP^{Sc}(P101L) with PTA in combination with cold PK digestion provides a new tool for dissecting the molecular mechanisms of inherited prion diseases. In addition, the results presented here coupled with an earlier report (29) argue that MoPrP(89-143, P101L) in a β-rich conformation triggers the generation of de novo GSS prions; indeed, our findings provide compelling evidence that this 55-mer mutant peptide folded into a β-rich structure is a synthetic prion.

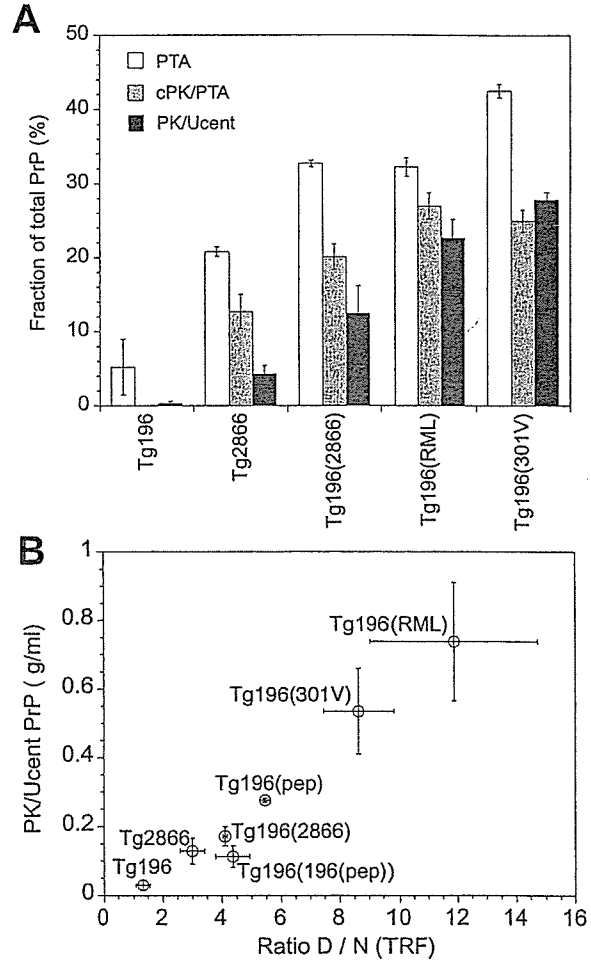

FIG. 6. Differential proteolytic resistance of aberrant, distinct PrP conformers in the brains of Tg(MoPrP,P101L) mice detected by the CDI. (A) Brain homogenates from spontaneously ill Tg(MoPrP, P101L)2866/*Prnp*$^{0/0}$ mice and Tg(MoPrP,P101L)196/*Prnp*$^{0/0}$ mice inoculated with RML prions, 301V prions, or GSS(P101L) prions from ill Tg2866 mice. Controls were age matched, uninoculated Tg mice. Samples were either left untreated (total PrP content), PTA precipitated, digested with cold PK followed by PTA precipitation (cPK/PTA), or digested with PK followed by ultracentrifugation (PK/Ucent). Results are shown as the fraction of total PrP recovered after each treatment. (B) Amount of $rPrP^{Sc}$ recovered after ultracentrifugation plotted as a function of the amount of antibody bound to the denatured and native forms of PrP (D:N ratio). Samples were obtained from the same mice depicted in panel A, in addition to Tg(MoPrP,P101L)196/*Prnp*$^{0/0}$ mice inoculated with the β-rich MoPrP(89-143,P101L) peptide on first [Tg196(pep)] and second [Tg196(196(pep))] passage. Data points and bars represent the means ± standard errors of the mean obtained from three independent measurements.

Synthetic prions. In an effort to construct a synthetic prion, we chose to focus our efforts on a genetic form of prion disease in order to bias the folding of PrP into a PrP^{Sc} isoform. Multiple attempts to generate prion infectivity from refolded recombinant PrPs have been unsuccessful to date (5–7). Since GSS(P102L) is the only inherited prion disease that has been successfully modeled in mice with respect to generating infectivity de novo, we chose to exploit the P102L mutation. To produce a synthetic prion, we constructed the 55-mer MoPrP (89-143,P101L) peptide using solid-phase peptide synthesis. When folded into a β-rich conformation, MoPrP(89-143, P101L) induced prion disease in Tg196 mice (Table 2) (29). The same peptide did not induce disease when it was not folded into a β-rich conformation. That the peptide must be in β-rich structure and the host must express MoPrP(P101L) in order to induce disease underscores the conformational specificity of prion propagation.

We report here that the disease induced in Tg196 mice by the β-rich MoPrP(89-143,P101L) peptide can be serially transmitted to Tg196 mice with an incubation time of ~350 days (Table 2). The presence of large multicentric plaques, which deposit in the neocortex, caudate nucleus, corpus callosum, hippocampus, and cerebellar cortex, together with focal vacuolar changes, corroborate the distinct characteristics of these GSS prions. From these experimental findings and those presented previously, we argue that the mutant 55-mer, β-rich peptide fulfills all of the criteria required for designation as a synthetic prion.

The neuropathologic changes characteristic of humans carrying the GSS(P102L) mutation, including large, multicentric plaques that stain with anti-PrP antibodies, are preserved in Tg(MoPrP,P101L) mice that develop prion disease spontaneously as well as in those that develop disease after inoculation with GSS prions or with the mutant 55-mer β-rich peptide. In contrast, when human GSS(P102L) prions are transmitted to nonhuman primates or non-Tg mice, these GSS-type plaques are rarely found (1, 32, 46). This distinction argues that the P→L substitution imposes a conformational constraint on host PrP^{C} that is required to preserve the disease characteristics of GSS.

It is noteworthy that polypeptides comprising the N domain of the yeast Sup35 protein have been expressed in *Escherichia coli* and folded into a β-rich conformation (3, 44). Such polypeptides readily polymerize into amyloid, which has been transferred into [PSI^{-}] *Saccharomyces cerevisiae* that in turn becomes [PSI^{+}], the prion state. As with the mutant 55-mer, β-rich peptide studies reported previously (29), these experiments with yeast argue for the production of a synthetic prion and contend that prions are composed only of protein, in accord with a wealth of other data (36).

Prion strains. Based on differences in resistance to limited proteolysis, two groups of prion strains can be distinguished: (i) those with low levels and (ii) those with high levels of $rPrP^{Sc}$ (P101L). Strains with low levels of $rPrP^{Sc}$(P101L) are formed spontaneously in Tg2866 mice and are formed in Tg196 mice after inoculation with either GSS(P101L) prions or the mutant 55-mer β-rich synthetic peptide. Prion strains with high levels of $rPrP^{Sc}$(P101L) were formed in Tg196 mice after inoculation with RML, 139A, or 301V prions. This last group of prion strains can be subdivided into two groups based on their incubation times in Tg196 mice: RML and 139A prions produce long incubation times, whereas 301V prions result in short incubation times. The P101L substitution in Tg196 mice introduced a transmission barrier and lengthened the incubation periods of RML and 139A prions (~180 days) compared to those observed in wt $Prnp^{a/a}$ mice (~130 days). In contrast, the replication of 301V prions in Tg196 mice did not encounter a transmission barrier, with incubation periods of ~125 days, similar to those found in $Prnp^{b/b}$ B6.I mice (Tables 2 and 3) (12). Since the phenomenon of transmission barriers induced by mutations was observed also in yeast prion [PSI^{+}], the mechanism appears to be a general paradigm for all prions regardless of the host or strain (17).

Conformational characteristics of PrP^{Sc}. The wide use of limited proteolysis to detect PrP 27-30 created the expectation that Tg(MoPrP,P101L) mice spontaneously developing CNS disease should possess readily detectable levels of mutant PrP 27-30 (15, 16). When PrP 27-30 was not found after limited PK digestion at 37°C, the modeling of GSS in Tg mice was thought to be unconvincing and prompted some investigators to doubt the interpretation of genetic linkage studies of humans carrying pathological mutations in the PrP gene.

In the studies reported here, we demonstrate that PrP^{Sc} conformers accumulate in the brains of Tg(MoPrP,P101L) mice that develop prion disease spontaneously as well as those that were inoculated with either GSS prions or the mutant 55-mer β-rich peptide. By modifying the conditions for limited proteolysis, we consistently demonstrated high levels of a disease-specific $sPrP^{Sc}$(P101L) conformer that generated PrP 22-24 upon cold PK digestion that was absent from the brains of wt mice (Table 1). Moreover, $sPrP^{Sc}$(P101L) accumulated in the brains of Tg2866 mice as a function of age and reached maximal levels when the mice displayed neurologic signs of prion disease (Fig. 5).

In the studies described here, PrP^{Sc}(P101L) adopted one conformation that was most readily detectable only after cold PK digestion and another conformation that was assayed by PK digestion at 37°C. Cold PK digestion demonstrated the presence of $sPrP^{Sc}$(P101L) in the brains of Tg2866 mice that develop prion disease spontaneously as well as of Tg196 mice that were inoculated with either GSS prions or the mutant 55-mer β-rich peptide (Fig. 3 to 5). PK digestion at 37°C was used to demonstrate $rPrP^{Sc}$(P101L) in the brains of Tg196 mice inoculated with prion strains derived from sheep with scrapie (RML and 139A prions) or cattle with BSE (301V prions) (Fig. 3C).

Defining the conformations of PrP^{Sc}(P101L) and wt PrP^{Sc} molecules promises to be difficult, since both are quite insoluble. Currently, the best approach to elucidating the structural features of wt PrP^{Sc} has been by electron crystallography of two-dimensional crystals (50). From the PK digestion studies of RML, 139A, and 301V prions propagated in Tg196 mice, it is reasonable to argue that $rPrP^{Sc}$(P101L) and wt $rPrP^{Sc}$ probably have similar structures. It is less clear how $sPrP^{Sc}$(P101L) in the brains of ill Tg2866 and Tg196 mice is related to wt $sPrP^{Sc}$. Assessing this relationship is difficult because no procedure has been developed to separate wt $sPrP^{Sc}$ from wt $rPrP^{Sc}$. Using the CDI, wt $sPrP^{Sc}$ can be calculated by subtracting PrP 27-30 from total PrP^{Sc}.

When the brains of Tg2866 mice were subjected to PK

digestion before or after PTA precipitation and inoculated into mice, the resulting incubation times were shorter than those obtained with untreated brain homogenates (Table 3), presumably reflecting increased titers due to the concentration of prions by selective PTA precipitation. Moreover, these results indicate that prion infectivity in the brains of Tg2866 mice is resistant to limited digestion with 25 μg of PK/ml for 1 h at 37°C. Similar resistance to proteolytic digestion was observed in the brains of Tg196 mice inoculated with either Tg2866 brain homogenates or 301V prions. The characteristics of different PrP isoforms are summarized in Table 1.

Mechanisms of neurodegeneration. Although there are many examples of modified PrP^C molecules, only PrP(P101L) has been shown to initiate an experimental prion disease that is transmissible. In studies using Tg mice, the expression of the D178N mutation did not produce neurologic deficits. The E200K and A117V mutations produced neurologic diseases, but brains from Tg mice carrying these mutations failed to transmit disease on passage in wt or isogenic hosts (24; P. Tremblay et al., unpublished observations). Similarly, the expression of a PrP transgene harboring an octapeptide repeat expansion from 5 to 14 repeats has been shown to initiate a spontaneous neurodegenerative condition similar to that observed in humans with prion disease (18, 19), but despite the accumulation of insoluble PrP conformers displaying low levels of protease resistance, the transmissibility of this disease has yet to be demonstrated. Expression of various designer mutations that led to the generation of PrP^C molecules with a transmembrane topology produced neurologic deficits correlating to the synthesis of topologically distinct, transmembrane PrP molecules (24, 25); again, attempts to transmit these diseases have failed (R. S. Hegde et al., unpublished observations). The general model emerging from all those experiments suggests that there are two probably independent misfolding pathways of mutant PrP: one leading to accumulation of misfolded conformers causing neurodegeneration and the other pathway leading to the accumulation of conformers that are infectious; whether the infectious conformers are also those that cause neurodegeneration remains to be established.

New directions in prion research. The discoveries reported here describe relatively crude biophysical correlations with prion infectivity generated in mice expressing MoPrP(P101L) transgenes. More detailed analyses might prove to be relevant in dissecting the mechanism of prion formation in the inherited prion diseases. The MoPrP(P101L) transgene has been unexpectedly useful in the study of prion strains. Coupled with new approaches using PTA precipitation and cold PK digestion, Tg mice expressing MoPrP(P101L) may increase our understanding of the mechanism by which prions are formed spontaneously as well as the structural features that encipher strain-specific information.

ACKNOWLEDGMENTS

This work was supported by grants from the National Institutes of Health (AG02132 and AG010770) and by a gift from the Leila Y. and G. Harold Mathers Charitable Foundation.

We thank the Hunter's Point Animal Facility.

REFERENCES

1. **Baker, H. F., L. W. Duchen, J. M. Jacobs, and R. M. Ridley.** 1990. Spongiform encephalopathy transmitted experimentally from Creutzfeldt-Jakob and familial Gerstmann-Sträussler-Scheinker diseases. Brain **113**:1891–1909.
2. **Baker, H. F., R. M. Ridley, and T. J. Crow.** 1985. Experimental transmission of an autosomal dominant spongiform encephalopathy: does the infectious agent originate in the human genome? Br. Med. J. **291**:299–302.
3. **Balbirnie, M., R. Grothe, and D. S. Eisenberg.** 2001. An amyloid-forming peptide from the yeast prion Sup35 reveals a dehydrated β-sheet structure for amyloid. Proc. Natl. Acad. Sci. USA **98**:2375–2380.
4. **Barry, R. A., and S. B. Prusiner.** 1986. Monoclonal antibodies to the cellular and scrapie prion proteins. J. Infect. Dis. **154**:518–521.
5. **Baskakov, I. V., C. Aagaard, I. Mehlhorn, H. Wille, D. Groth, M. A. Baldwin, S. B. Prusiner, and F. E. Cohen.** 2000. Self-assembly of recombinant prion protein of 106 residues. Biochemistry **39**:2792–2804.
6. **Baskakov, I. V., G. Legname, M. A. Baldwin, S. B. Prusiner, and F. E. Cohen.** 2002. Pathway complexity of prion protein assembly into amyloid. J. Biol. Chem. **277**:21140–21148.
7. **Baskakov, I. V., G. Legname, S. B. Prusiner, and F. E. Cohen.** 2001. Folding of prion protein to its native α-helical conformation is under kinetic control. J. Biol. Chem. **276**:19687–19690.
8. **Bolton, D. C., M. P. McKinley, and S. B. Prusiner.** 1982. Identification of a protein that purifies with the scrapie prion. Science **218**:1309–1311.
9. **Brown, P., C. J. Gibbs, Jr., P. Rodgers-Johnson, D. M. Asher, M. P. Sulima, A. Bacote, L. G. Goldfarb, and D. C. Gajdusek.** 1994. Human spongiform encephalopathy: the National Institutes of Health series of 300 cases of experimentally transmitted disease. Ann. Neurol. **35**:513–529.
10. **Bruce, M., A. Chree, I. McConnell, J. Foster, G. Pearson, and H. Fraser.** 1994. Transmission of bovine spongiform encephalopathy and scrapie to mice: strain variation and the species barrier. Phil. Trans. R. Soc. Lond. B **343**:405–411.
11. **Büeler, H., M. Fisher, Y. Lang, H. Bluethmann, H.-P. Lipp, S. J. DeArmond, S. B. Prusiner, M. Aguet, and C. Weissmann.** 1992. Normal development and behaviour of mice lacking the neuronal cell-surface PrP protein. Nature **356**:577–582.
12. **Carlson, G. A., C. Ebeling, S.-L. Yang, G. Telling, M. Torchia, D. Groth, D. Westaway, S. J. DeArmond, and S. B. Prusiner.** 1994. Prion isolate specified allotypic interactions between the cellular and scrapie prion proteins in congenic and transgenic mice. Proc. Natl. Acad. Sci. USA **91**:5690–5694.
13. **Carlson, G. A., D. T. Kingsbury, P. A. Goodman, S. Coleman, S. T. Marshall, S. DeArmond, D. Westaway, and S. B. Prusiner.** 1986. Linkage of prion protein and scrapie incubation time genes. Cell **46**:503–511.
14. **Chandler, R. L.** 1961. Encephalopathy in mice produced by inoculation with scrapie brain material. Lancet **i**:1378–1379.
15. **Chesebro, B.** 1998. Prion diseases: BSE and prions: uncertainties about the agent. Science **279**:42–43.
16. **Chesebro, B.** 1992. PrP and the scrapie agent. Nature **356**:560.
17. **Chien, P., A. H. DePace, S. R. Collins, and J. S. Weissman.** 2003. Generation of prion transmission barriers by mutational control of amyloid conformations. Nature **424**:948–951.
18. **Chiesa, R., B. Drisaldi, E. Quaglio, A. Migheli, P. Piccardo, B. Ghetti, and D. A. Harris.** 2000. Accumulation of protease-resistant prion protein (PrP) and apoptosis of cerebellar granule cells in transgenic mice expressing a PrP insertional mutation. Proc. Natl. Acad. Sci. USA **97**:5574–5579.
19. **Chiesa, R., P. Piccardo, B. Ghetti, and D. A. Harris.** 1998. Neurological illness in transgenic mice expressing a prion protein with an insertional mutation. Neuron **21**:1339–1351.
20. **DeArmond, S. J., and J. W. Ironside.** 1999. Neuropathology of prion diseases, p. 585–652. *In* S. B. Prusiner (ed.), Prion biology and diseases. Cold Spring Harbor Laboratory Press, Cold Spring Harbor, N.Y.
21. **Dickinson, A. G.** 1976. Scrapie in sheep and goats, p. 209–241. *In* R. H. Kimberlin (ed.), Slow virus diseases of animals and man. North-Holland Publishing, Amsterdam, The Netherlands.
22. **Fraser, H., M. E. Bruce, A. Chree, I. McConnell, and G. A. H. Wells.** 1992. Transmission of bovine spongiform encephalopathy and scrapie to mice. J. Gen. Virol. **73**:1891–1897.
23. **Gambetti, P., R. B. Peterson, P. Parchi, S. G. Chen, S. Capellari, L. Goldfarb, R. Gabizon, P. Montagna, E. Lugaresi, P. Piccardo, and B. Ghetti.** 1999. Inherited prion diseases, p. 509–583. *In* S. B. Prusiner (ed.), Prion biology and diseases. Cold Spring Harbor Laboratory Press, Cold Spring Harbor, N.Y.
24. **Hegde, R. S., J. A. Mastrianni, M. R. Scott, K. A. DeFea, P. Tremblay, M. Torchia, S. J. DeArmond, S. B. Prusiner, and V. R. Lingappa.** 1998. A transmembrane form of the prion protein in neurodegenerative disease. Science **279**:827–834.
25. **Hegde, R. S., P. Tremblay, D. Groth, S. B. Prusiner, and V. R. Lingappa.** 1999. Transmissible and genetic prion diseases share a common pathway of neurodegeneration. Nature **402**:822–826.
26. **Hsiao, K., M. Scott, D. Foster, S. J. DeArmond, and S. B. Prusiner.** 1990. Towards a model of Gerstmann-Sträussler-Scheinker syndrome in transgenic mice. Soc. Neurosci. Abstr. **16**(part 2):1138.
27. **Hsiao, K. K., D. Groth, M. Scott, S.-L. Yang, H. Serban, D. Rapp, D. Foster, M. Torchia, S. J. DeArmond, and S. B. Prusiner.** 1994. Serial transmission in rodents of neurodegeneration from transgenic mice expressing mutant prion protein. Proc. Natl. Acad. Sci. USA **91**:9126–9130.
28. **Hsiao, K. K., M. Scott, D. Foster, D. F. Groth, S. J. DeArmond, and S. B.**

Prusiner. 1990. Spontaneous neurodegeneration in transgenic mice with mutant prion protein. Science 250:1587–1590.
29. Kaneko, K., H. L. Ball, H. Wille, H. Zhang, D. Groth, M. Torchia, P. Tremblay, J. Safar, S. B. Prusiner, S. J. DeArmond, M. A. Baldwin, and F. E. Cohen. 2000. A synthetic peptide initiates Gerstmann-Sträussler-Scheinker (GSS) disease in transgenic mice. J. Mol. Biol. 295:997–1007.
30. Kascsak, R. J., R. Rubenstein, P. A. Merz, M. Tonna-DeMasi, R. Fersko, R. I. Carp, H. M. Wisniewski, and H. Diringer. 1987. Mouse polyclonal and monoclonal antibody to scrapie-associated fibril proteins. J. Virol. 61:3688–3693.
31. Manson, J. C., E. Jameison, H. Baybutt, N. L. Tuzi, R. Barron, I. McConnell, R. Somerville, J. Ironside, R. Will, M.-S. Sy, D. W. Melton, J. Hope, and C. Bostock. 1999. A single amino acid alteration (101L) introduced into murine PrP dramatically alters incubation time of transmissible spongiform encephalopathy. EMBO J. 18:6855–6864.
32. Masters, C. L., D. C. Gajdusek, and C. J. Gibbs, Jr. 1981. Creutzfeldt-Jakob disease virus isolations from the Gerstmann-Sträussler syndrome. Brain 104: 559–588.
33. Moore, R. C., J. Hope, P. A. McBride, I. McConnell, J. Selfridge, D. W. Melton, and J. C. Manson. 1998. Mice with gene targetted prion protein alterations show that *Prnp*, Sinc and *Prni* are congruent. Nat. Genet. 18:118–125.
34. Muramoto, T., S. J. DeArmond, M. Scott, G. C. Telling, F. E. Cohen, and S. B. Prusiner. 1997. Heritable disorder resembling neuronal storage disease in mice expressing prion protein with deletion of an α-helix. Nat. Med. 3:750–755.
35. Peretz, D., R. A. Williamson, Y. Matsunaga, H. Serban, C. Pinilla, R. B. Bastidas, R. Rozenshteyn, T. L. James, R. A. Houghten, F. E. Cohen, S. B. Prusiner, and D. R. Burton. 1997. A conformational transition at the N-terminus of the prion protein features in formation of the scrapie isoform. J. Mol. Biol. 273:614–622.
36. Prusiner, S. B. 1998. Prions. Proc. Natl. Acad. Sci. USA 95:13363–13383.
37. Prusiner, S. B., D. C. Bolton, D. F. Groth, K. A. Bowman, S. P. Cochran, and M. P. McKinley. 1982. Further purification and characterization of scrapie prions. Biochemistry 21:6942–6950.
38. Prusiner, S. B., S. P. Cochran, D. F. Groth, D. E. Downey, K. A. Bowman, and H. M. Martinez. 1982. Measurement of the scrapie agent using an incubation time interval assay. Ann. Neurol. 11:353–358.
39. Safar, J., H. Wille, V. Itri, D. Groth, H. Serban, M. Torchia, F. E. Cohen, and S. B. Prusiner. 1998. Eight prion strains have PrP^{Sc} molecules with different conformations. Nat. Med. 4:1157–1165.
40. Safar, J. G., M. Scott, J. Monaghan, C. Deering, S. Didorenko, J. Vergara, H. Ball, G. Legname, E. Leclerc, L. Solforosi, H. Serban, D. Groth, D. R. Burton, S. B. Prusiner, and R. A. Williamson. 2002. Measuring prions causing bovine spongiform encephalopathy or chronic wasting disease by immunoassays and transgenic mice. Nat. Biotechnol. 20:1147–1150.
41. Scott, M., D. Foster, C. Mirenda, D. Serban, F. Coufal, M. Wälchli, M. Torchia, D. Groth, G. Carlson, S. J. DeArmond, D. Westaway, and S. B. Prusiner. 1989. Transgenic mice expressing hamster prion protein produce species-specific scrapie infectivity and amyloid plaques. Cell 59:847–857.
42. Scott, M. R., R. Will, J. Ironside, H.-O. B. Nguyen, P. Tremblay, S. J. DeArmond, and S. B. Prusiner. 1999. Compelling transgenetic evidence for transmission of bovine spongiform encephalopathy prions to humans. Proc. Natl. Acad. Sci. USA 96:15137–15142.
43. Serban, D., A. Taraboulos, S. J. DeArmond, and S. B. Prusiner. 1990. Rapid detection of Creutzfeldt-Jakob disease and scrapie prion proteins. Neurology 40:110–117.
44. Sparrer, H. E., A. Santoso, F. C. Szoka, Jr., and J. S. Weissman. 2000. Evidence for the prion hypothesis: induction of the yeast [*PSI*$^+$] factor by in vitro-converted Sup35 protein. Science 289:595–599.
45. Taraboulos, A., K. Jendroska, D. Serban, S.-L. Yang, S. J. DeArmond, and S. B. Prusiner. 1992. Regional mapping of prion proteins in brains. Proc. Natl. Acad. Sci. USA 89:7620–7624.
46. Tateishi, J., T. Kitamoto, M. Z. Hoque, and H. Furukawa. 1996. Experimental transmission of Creutzfeldt-Jakob disease and related diseases to rodents. Neurology 46:532–537.
47. Telling, G. C., T. Haga, M. Torchia, P. Tremblay, S. J. DeArmond, and S. B. Prusiner. 1996. Interactions between wild-type and mutant prion proteins modulate neurodegeneration in transgenic mice. Genes Dev. 10:1736–1750.
48. Telling, G. C., M. Scott, J. Mastrianni, R. Gabizon, M. Torchia, F. E. Cohen, S. J. DeArmond, and S. B. Prusiner. 1995. Prion propagation in mice expressing human and chimeric PrP transgenes implicates the interaction of cellular PrP with another protein. Cell 83:79–90.
49. Westaway, D., P. A. Goodman, C. A. Mirenda, M. P. McKinley, G. A. Carlson, and S. B. Prusiner. 1987. Distinct prion proteins in short and long scrapie incubation period mice. Cell 51:651–662.
50. Wille, H., M. D. Michelitsch, V. Guénebaut, S. Supattapone, A. Serban, F. E. Cohen, D. A. Agard, and S. B. Prusiner. 2002. Structural studies of the scrapie prion protein by electron crystallography. Proc. Natl. Acad. Sci. USA 99:3563–3568.

Available online at www.sciencedirect.com

SCIENCE DIRECT®

Brain Research 1019 (2004) 1–9

BRAIN RESEARCH

www.elsevier.com/locate/brainres

Research report

Accumulation of β- and γ-synucleins in the ubiquitin carboxyl-terminal hydrolase L1-deficient *gad* mouse

Yu-Lai Wang[a], Ayako Takeda[a], Hitoshi Osaka[a,b], Yoko Hara[a], Akiko Furuta[a], Rieko Setsuie[a,c], Ying-Jie Sun[a], Jungkee Kwon[a,d], Yae Sato[a,c], Mikako Sakurai[a,c], Mami Noda[c], Yasuhiro Yoshikawa[d], Keiji Wada[a,*]

[a] *Department of Degenerative Neurological Diseases, National Institute of Neuroscience, National Center of Neurology and Psychiatry, Kodaira, Tokyo 187-8502, Japan*

[b] *Information and Cellular Function, PRESTO, Japan Science and Technology Agency (JST), Kawaguchi, Saitama 332-0012, Japan*

[c] *Laboratory of Pathophysiology, Graduate School of Pharmaceutical Sciences, Kyushu University, Higashi, Fukuoka, 812-8582, Japan*

[d] *Department of Biomedical Science, Graduate School of Agricultural and Life Sciences, University of Tokyo, 1-1-1 Yayoi, Bunkyo, Tokyo, 113-8657, Japan*

Accepted 11 May 2004

Abstract

The synuclein family includes three isoforms, termed α, β and γ. α-Synuclein accumulates in various pathological lesions resulting from neurodegenerative disorders including Parkinson's disease (PD), dementia with Lewy bodies (DLB) and multiple system atrophy. However, neither β- nor γ-synuclein has been detected in Lewy bodies, and thus it is unclear whether these isoforms contribute to neurological pathology. In the present study, we used immunohistochemistry to demonstrate accelerated accumulation of β- and γ-synucleins in axonal spheroids in gracile axonal dystrophy (*gad*) mice, which do not express ubiquitin carboxyl-terminal hydrolase L1 (UCH-L1). γ-Synuclein immunoreactivity in the spheroids appeared in the gracile nucleus at 3 weeks of age and was maintained until 32 weeks. β-Synuclein immunoreactivity appeared in spheroids around 12 weeks of age. In contrast, α-synuclein immunoreactivity was barely detectable in spheroids. Immunoreactivity for synaptophysin and ubiquitin were either faint or undetectable in spheroids. Given that UCH-L1 deficiency results in axonal degeneration and spheroid formation, our findings suggest that β- and γ-synuclein participate in the pathogenesis of axonal swelling in *gad* mice.

Theme: Disorders of the nervous system
Topic: Degenerative disease: other

Keywords: Synuclein; Spheroid; UCH-L1; Ubiquitin

1. Introduction

The synucleins are a family of small cytosolic proteins that are expressed abundantly in the nervous system. Their contribution to neurophysiological function, however, is poorly understood. The mouse synuclein family consists of three members, α-synuclein (α-syn), β-synuclein (β-syn) and γ-synuclein (γ-syn), which range from 123 to 140 residues in length, exhibit 48–58% amino acid sequence identity and share similar domain organization (Fig. 1). Immunohistochemistry in the normal brain shows that α- and β-syn are concentrated at nerve terminals with little staining of somata and dendrites. Ultrastructural studies show that these isoforms localize to nerve terminals in close proximity to synaptic vesicles [18]. In contrast, γ-syn is present throughout nerve cells and is most abundant in the peripheral nervous system [5,18].

The synuclein family has been implicated in neurodegenerative diseases. Two point mutations (A53T, A30P) in the gene encoding α-synuclein (*SNCA*) have been detected in two distinct Parkinson's disease (PD) sibships with autosomal dominant inheritance [17,26], and a heritable

* Corresponding author. Tel.: +81-42-346-1715; fax: +81-42-346-1745.
E-mail address: wada@ncnp.go.jp (K. Wada).

0006-8993/$ - see front matter © 2004 Elsevier B.V. All rights reserved.
doi:10.1016/j.brainres.2004.05.023

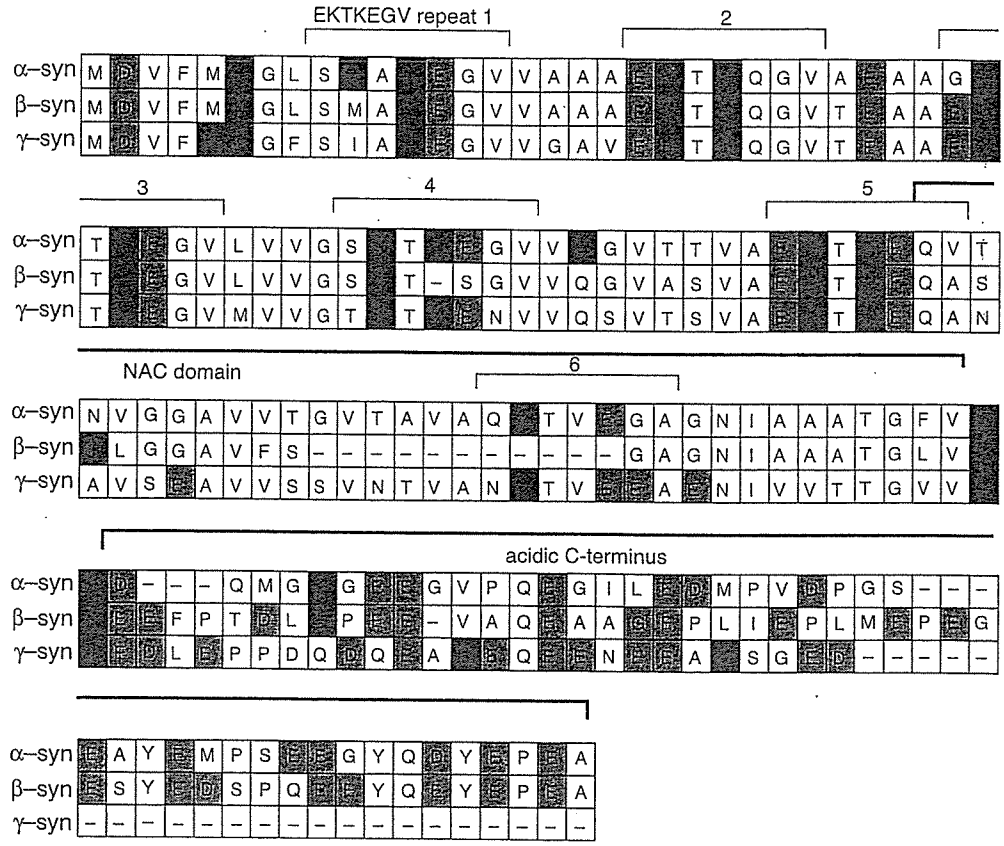

Fig. 1. Comparison of amino acid sequences from mouse α-, β- and γ-synuclein. The N-terminal region contains six imperfect repeats of the consensus EKTKEGV and the C-terminal region is negatively charged. A part of the hydrophobic NAC (non-amyloid component of amyloid plaque) domain is deleted in β-syn. Basic and acidic residues are shown in blue and red, respectively. Sequence accession numbers: mouse α-syn, NP-033247; mouse β-syn, NP-291088; mouse γ-syn, NP-035560.

genomic triplication of *SNCA* has been described within two distinct families [6,33]. Also, α-synuclein protein is a primary component of Lewy bodies (intracellular inclusions) and accumulates in abnormal neurites that contain ubiquitin, synaptophysin and neurofilaments [9,36,37]. β-Syn and γ-syn, which is also known as breast cancer-specific gene 1 (*BCSGI*), are overexpressed in neurodegenerative diseases such as PD and dementia with Lewy bodies (DLB) [5,7]. Unlike α- and β-syn, γ-syn is distributed throughout the cytoplasm of neurons where it influences the integration of neurofilament networks [4].

Ubiquitin carboxyl-terminal hydrolase L1 (UCH-L1) has been found throughout the brain and testis/ovary and has been considered as plays an important role in the labeling of abnormal proteins in the ubiquitin-proteasome system [15,38]. The gracile axonal dystrophy (*gad*) mouse is an autosomal recessive spontaneous mutant that was identified in 1984 [42]. It is the first mammalian neurological model with a defect in the ubiquitin-proteasome system [28]. These mice carry an intragenic deletion of the UCH-L1 gene (*Uchl1*) and do not express UCH-L1, making them comparable to a *Uchl1* null mutant [24,28]. The *gad* mouse exhibits severe sensory ataxia at an early stage, followed by motor paresis at a later stage [14,42]. In the central nervous system of *gad* mice, axonal degeneration begins from the distal ends of primary ascending axons in the dorsal root ganglia (DRG) [21,22]. Spheroid formation with the dying-back type of axonal degeneration is first observed in the gracile and dorsal spinocerebellar tracts [14,21,42]. In the most rostral portion of the gracile fascicles, spheroids are observed around 12 weeks of age and their formation progresses gradually to the terminal stage after 20 weeks of age [22]. At a later stage, axonal degeneration and spheroid formation are observed in the upper tracts of DRG neurons as well as in motor neurons [22]. Although the *gad* mutation is known to be caused by a deficiency in UCH-L1, the mechanism of spheroid formation is not well understood. Dystrophic axons or axonal spheroids have been observed in the brains of patients with infantile neuroaxonal dystrophy [1], in the globus pallidus in Hallervorden-Spatz disease [10], and in the gracile and cuneate nuclei in human vitamin-E deficiency [29]. Furthermore, spheroids are often observed in the medulla and spinal cords of aged mammals. In normal mice, the number of spheroids increases with age in the gracile nucleus [43].

Components of the spheroids of *gad* mice include amyloid-β protein, mitochondria, neurofilaments and synaptic complexes [12,22]. Ubiquitin and amyloid-β protein

also accumulate outside spheroids along the sensory and motor nervous systems [12,40]. We previously observed dot-like deposits of ubiquitin immunoreactivity throughout the gracile nucleus [40]. These data led us to suggest that the absence of functional UCH-L1 may affect the hydrolysis of unknown substrates, which could result in the formation of protein aggregates. α-Syn accumulation has been detected in spheroids resulting from type 1 iron accumulation in the brain (NBIA 1), a rare neurodegenerative disorder characterized by axonal spheroids and Lewy body-like intraneuronal inclusions [8]. Moreover, β-syn and γ-syn immunoreactivity were detected in spheroids but not in Lewy body-like inclusions [8]. In PD and DLB, axonal spheroid-like lesions were identified in the molecular layer of the dentate gyrus along with the accumulation of γ-syn, but not of α- or β-syn [7].

In the present study, we investigated the accumulation of α-syn, β-syn and γ-syn in the *gad* mouse using isoform-specific antibodies. Unexpectedly, we did not detect α-syn in spheroids, although β-syn and γ-syn accumulated in these structures beginning at an early stage of pathology. These results demonstrate that the *gad* mouse constitutes a useful model for investigating the role of synucleins in neurodegeneration.

2. Materials and methods

2.1. Animals

All mice were maintained and propagated at our institute. Adult homozygous *gad/gad* and wild-type (+/+) mice were obtained by mating heterozygous males with heterozygous females. All mouse experiments were performed in accordance with our institution's regulations for animal care and with the approval of the Animal Investigation Committee of the National Institute of Neuroscience, National Center of Neurology and Psychiatry. Each experimental group consisted of three male mice of the same phenotype, and experiments were conducted at 3 weeks (initial stage), 12 weeks (progressive stage), 17 and 20 weeks (critical stage), and 32 weeks (terminal stage) after birth [44].

2.2. Histochemistry

Mice were anesthetized and perfused with 0.9% NaCl followed by ice-cold 4% paraformaldehyde in phosphate-buffered saline (PBS, pH 7.4). Brains and spinal cords were then collected and postfixed in 4% paraformaldehyde overnight at 4 °C. The medulla oblongata and the upper cervical cord were examined. To ensure near complete concordance in the anatomical level of each sample, we followed the Atlas of the Mouse Brain and Spinal Cord [32]. Coronal sections were made at the level of the gracile nucleus (level 535) and of the cervical (C3) spinal cord segments. The samples were embedded in paraffin and sectioned (4 μm) for immunostaining and light microscopy. All sections from mice of the same age group were processed in parallel for each marker. Some sections were stained with hematoxylin–eosin (HE) and Klüver-Barrera for examination by conventional pathological methods. Quantification using stereological techniques was performed by counting eosinophilic spheroids at the medulla and upper cervical levels in at least three sections per sample by two blind observers. We then calculated the average number of spheroids per section. Spheroids were counted using the 200× lens of a Zeiss Axioplan microscope. Under this magnification, eosinophilic spheroids are clearly viewed.

For immunohistochemistry, serial sections were deparaffinized in xylene and graded ethanol, washed in distilled water, and then treated with 0.3% H_2O_2 in methanol for 30 min to quench endogenous peroxidase activity. For the enhancement of α-syn immunostaining, sections were pretreated with 99% formic acid for 5 min or autoclaved at 121 °C for 10 min [35,36]. The sections were washed three times for 5 min in PBS, and then nonspecific binding sites were blocked by incubation in 10% normal serum obtained from the species in which the secondary antibody was generated. After a brief rinse with PBS, sections were incubated overnight at 4 °C with primary antibodies. Primary and secondary antibodies were diluted in DAKO Antibody Diluent (Dako, CA). The following antibodies were used at the final dilutions indicated: monoclonal α-syn antibody (1:100; BD Transduction Laboratories, CA), polyclonal β-syn antibody (1:200; Affinity Research Products), monoclonal synaptophysin antibody (1:50; Dako) and polyclonal ubiquitin antibody (1:400; Chemicon, Temecula). Polyclonal γ-syn antibody (see below) was diluted 1:100.

Subsequent antibody detection was carried out using anti-rabbit or anti-mouse IgG from the VECTASTAIN Elite ABC kit (Vector Labs, Burlingame, CA). Briefly, after washing, sections were sequentially incubated with biotinylated secondary antibodies for 1 h followed by avidin–biotin complex (diluted 1:200) for 1 h. Bound antibody complexes were visualized using 3,3′-diaminobenzidine tetrachloride as a peroxidase substrate. Sections were then lightly counterstained with hematoxylin. For the blocking experiments, anti-γ-syn was initially incubated with recombinant γ-syn for 4 h at 4 °C and the staining procedure was then performed as described above. The sections from different groups were immunostained and treated at the same time. For controls, the primary antibody was replaced with normal rabbit serum or was omitted (these controls always yielded negative staining).

2.3. Preparation of γ-syn antibody and antibody purification

γ-Syn cDNA was cloned from mouse brain mRNA using PCR with a primer set designed using the γ-syn nucleotide

sequence in GenBank (AF017255; sense primer, 5′-ACATG-CATGCGACGTCTTCAAGAAAGGCTTC-3′; antisense primer, 5′-CCCAAGCTTGTCTTCTCCACTCTTGGC-3′). The γ-syn cDNA was cloned into the expression vector pEQ-30 (Qiagen, Germany), yielding a recombinant plasmid used to express histidine-tagged γ-syn (6-His-γ-syn) in *E. coli*. Recombinant 6-His-γ-syn was prepared as previously described [23] and used to generate a polyclonal antiserum in rabbits (Takara, Japan). The polyclonal antibodies were purified by affinity chromatography according to the manufacturer's instructions.

2.4. Specificities of synuclein antibodies

Purified recombinant α-syn (BD Transduction Laboratories), β-syn (Alpha Diagnostic International, TX) and γ-syn were diluted and subjected to electrophoresis through SDS-polyacrylamide gels (15% acrylamide) at 200, 100, 50, 25 and 12.5 ng per lane for each protein. The proteins were electrophoretically transferred to PVDF membranes (Bio-Rad, CA) as previously reported [23]. For immunochemical detection of the proteins, the membranes were first blocked in Tris-buffered saline containing 0.1% (w/v) Tween 20 (TTBS) and 3% BSA overnight at 4 °C and then incubated for 12 h with anti-α-syn (1:1000) or with anti-β- or anti-γ-syn (1:500). Antibodies were diluted in DAKO Antibody Diluent. The membranes were washed with TTBS and then incubated with horseradish peroxidase (HRP)-conjugated goat anti-rabbit or anti-mouse IgG (1:10,000; Pierce, IL) for 1 h. Proteins were detected using the SuperSignal chemiluminescence system (Pierce).

3. Results

3.1. Histopathological analysis of the gracile nucleus by HE staining

Oval or round spheroids were visualized by HE staining of axonal sections from wild-type mice at 20 weeks of age. However, fewer than five spheroids per section were detected. In contrast, gracile nuclei of *gad* mice exhibited both axonal dystrophy and spheroids as early as 3 weeks of age (Fig. 2A), in agreement with a previous report [44]. The number of spheroids increased with age, and the HE staining intensity of spheroids was relatively high until 20 weeks of age (Fig. 2B,C) but was very faint at 32 weeks (Fig. 2D). The size and appearance of the spheroids detected in *gad* mice varied with age. Irregularly shaped spheroids were observed from 12 to 20 weeks, whereas other spheroids stained diffusely or granularly as observed in wild-type mice (Fig. 2E). Some spheroids displayed an intense eosinophilic core, vacuoles or thin clefts (Fig. 2B).

We manually counted the total number of spheroids in the dorsal columns and dorsal nuclei of the medulla and upper cervical spinal cord using stereological techniques. Spheroids were detected in *gad* mice at all ages examined (Fig. 2F). The number of spheroids increased with age until 20 weeks (mean ± S.D.; $n = 8 \sim 13$): 3 weeks, 3.2 ± 0.8; 12 weeks, 12.1 ± 3.4; 20 weeks, 16.3 ± 3.9. At 32 weeks, however, the number of spheroids decreased (7.8 ± 2.2), as did their size (data not shown). These observations most likely reflect the severity of degeneration following the progression of the dying-back type of axonal dystrophy [14,44] to the lower spinal cord. In comparison, only a very

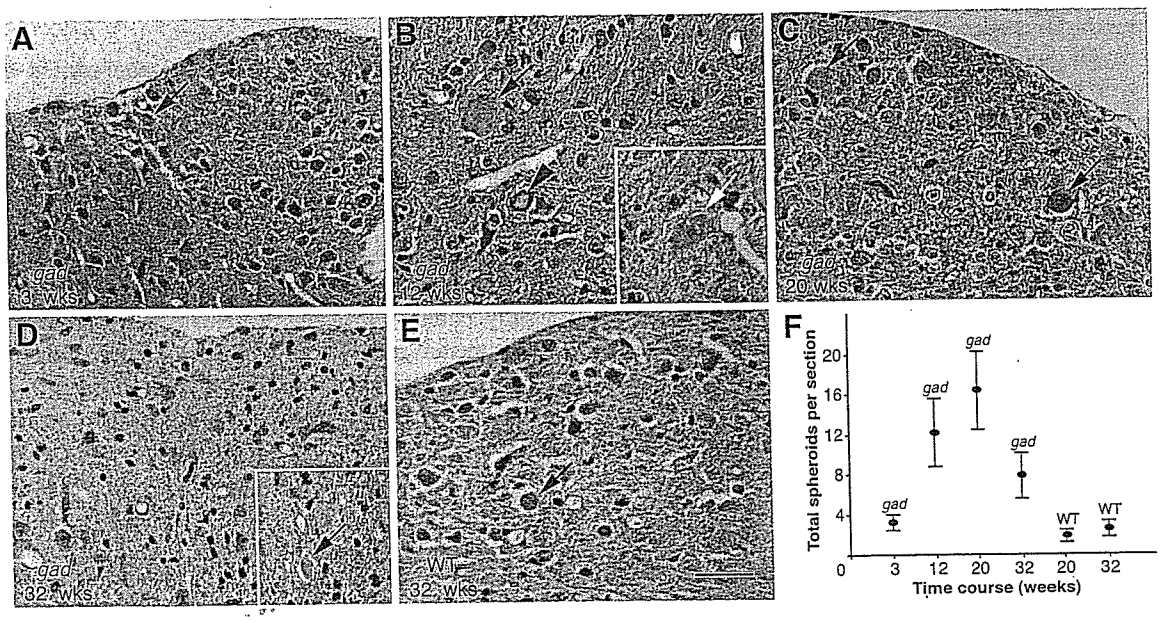

Fig. 2. Hematoxylin–eosin staining of eosinophilic spheroids (arrows) in (A–D) gad sections of the gracile nucleus of the medulla oblongata at 3, 12, 20 and 32 weeks of age, respectively, and in (E) a wild-type section at 32 weeks. An arrowhead indicates a vacuolar spheroid body, and a white arrow indicates a spheroid with an intense eosinophilic core (inset in B). (F) A quantitative study of spheroid number over time in gad and WT mice. Values are the mean ± S.D. ($n = 8 \sim 13$). Bar = 50 μm.

small number of spheroids were found in wild-type mice (1.8±0.6 at 20 weeks, 2.5 ± 0.8 at 32 weeks; $n=9$; Fig. 2F).

3.2. Spheroids of gad mice accumulate β-syn and γ-syn but lack α-syn

We tested the specificity of the synuclein antibodies using purified recombinant synuclein isoforms. Polyclonal anti-γ-syn recognized purified recombinant γ-syn but did not cross-react with recombinant α-syn or β-syn in western blots (Fig. 3C). This antibody was also useful for immunohistochemical detection of γ-syn in spheroids in the gracile nucleus (Fig. 4A–D). No staining was observed when polyclonal anti-γ-syn was pre-absorbed with recombinant γ-syn (1:20 antibody/protein molar ratio; data not shown), thereby demonstrating the specificity of the staining. Under the same conditions, controls without anti-γ-syn showed no immunoreactivity (data not shown). An assay of specificity was also performed using the commercial antibodies against α-syn and β-syn, and similar results were obtained for both antibodies (Fig. 3A,B).

We then utilized all three isoform-specific antibodies to characterize the pathology of axonal degeneration in the *gad* mouse. Immunoreactivity to γ-syn was robust during postnatal weeks 3 ~ 20 but was weak at week 32 (Table 1). At 3 weeks of age, the spheroids detected by anti-γ-syn were more clearly recognized than those detected by HE staining. γ-Syn-immunoreactive spheroids varied in appearance as shown by HE staining (Fig. 2A–D), and oval or round spheroids were often diffusely or granularly immunostained by anti-γ-syn (Fig. 4A–C). Numerous dystrophic axons also displayed γ-syn immunoreactivity. γ-Syn immunoreactivity was absent both in spheroids and dystrophic axons when anti-γ-syn was pre-incubated with excess purified γ-syn (data not shown). In contrast to γ-syn immunoreactivity, spheroids started to exhibit faint and sporadic β-syn immunostaining from 12 weeks of age, with the intensity increasing through 32 weeks (Fig. 4E,F and Table 1). At 32 weeks, relatively intense β-syn staining was observed in spheroids and dystrophic axons (Fig. 4G); however, there were fewer immunopositive spheroids than were seen by γ-syn staining (at 20 weeks; Fig. 4C). Coarse granules around neurons were also immunostained by anti-β-syn (Fig. 4G). Very little α-syn immunoreactivity was observed in spheroids even after enhancement with formic acid or by autoclaving (Fig. 4I). These pretreatments also failed to show α-syn immunoreactivity in axons (Fig. 4I).

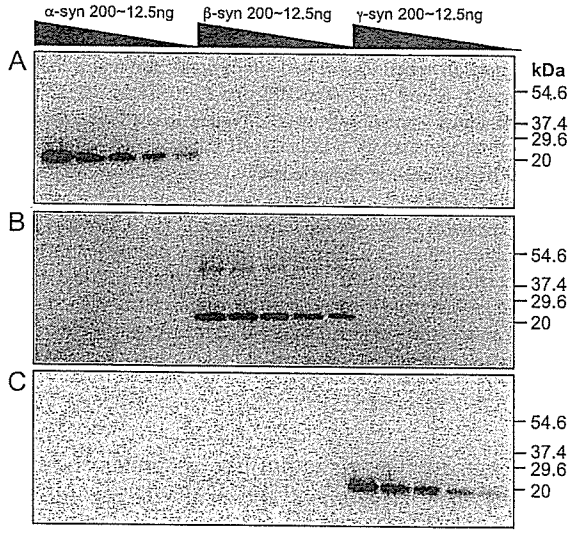

Fig. 3. Specificity of synuclein antibodies. Western blots show the specificity and reactivity of anti-α-syn, anti-β-syn and anti-γ-syn with varying amounts (12.5 ~ 200 ng) of all three recombinant synucleins. Three identical SDS-polyacrylamide gels were transferred to membranes under identical conditions, and each membrane was then probed separately with one of the synuclein antibodies. (A) α-syn antibody. (B) β-syn antibody. (C) γ-syn antibody. None of the antibodies exhibited significant cross-reactivity. A dimer formation (~ 50 kDa) was seen in the β-syn blot (B). Molecular weight markers (in kDa) are shown to the right.

In wild-type mice, spheroids were immunopositive for γ-syn (Fig. 4D) and β-syn (a relatively weak punctate pattern in the center of spheroids; Fig. 4H). However, no α-syn immunoreactivity was detected (Fig. 4J, arrows). Also, ubiquitin-positive immunostaining, which did not appear until 20 weeks, was seen in spheroids and as dots that did not correspond to spheroids (data not shown). In *gad* mice, ubiquitin-immunoreactive dots appeared from 12 weeks of age as previously demonstrated [40] and spheroids were not immunoreactive for ubiquitin (Fig. 4K). Ubiquitin staining in general was more intense in the wild-type tissue (Fig. 4L) than in *gad* tissue (Fig. 4K). For synaptophysin, the limited number of spheroids were immunopositive in both wild-type and *gad* mice at 20 weeks of age, with a diffuse or spotty staining in the center of the spheroids (Fig. 4M,O). The *gad* mouse appears to show higher synaptophysin expression than wild-type mice (Fig. 4M,O). At 32 weeks, *gad* mice displayed a punctate distribution pattern of synaptophysin along synapses or surrounding cell bodies with a few densely stained spheroids (Fig. 4N, arrow). In contrast, wild-type mice displayed an expression pattern that was enriched in the spheroids at 32 weeks of age (Fig. 4P, arrow). Furthermore, *gad* mice exhibited dot-like immunostaining for ubiquitin (Fig. 4L, arrowheads), β-syn (Fig. 4G) and γ-syn (Fig. 4C).

4. Discussion

Previous studies of *gad* mice showed axonal degeneration and spheroid-formation (axonal dystrophy) in the gracile tract during the initial stage of neuropathology [14,22,44]. During the critical stage from 17 to 20 weeks of age, the pathological changes extend to the spinocerebellar tract and spinal trigeminal nucleus. During the terminal stage (beyond 32 weeks), these changes extend to the corticospinal tract, cuneate tract, spinal trigeminal tract and thalamus [44]. Although synucleins have been implicated in the pathology of various neurodegenerative disorders, the

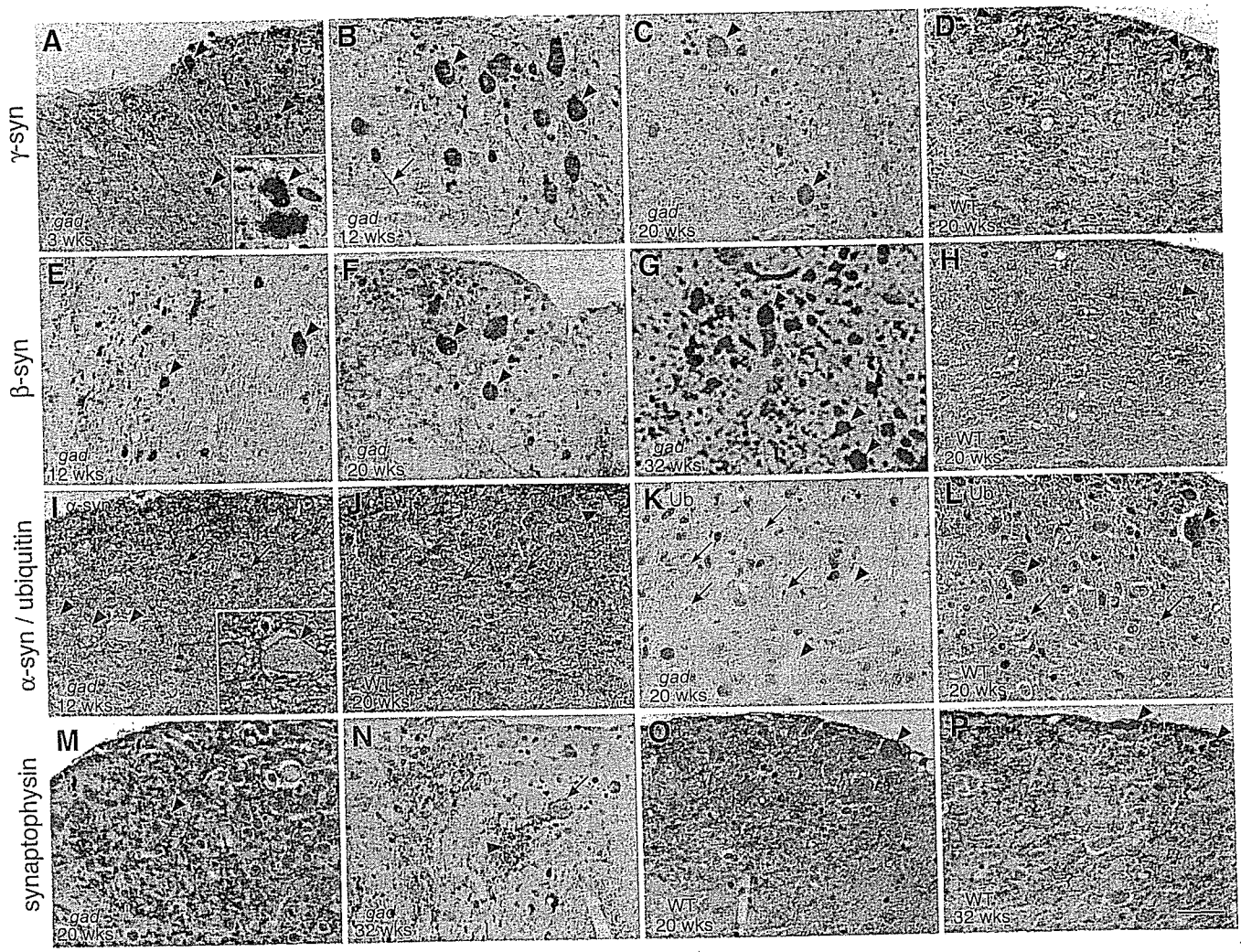

Fig. 4. Synucleins, synaptophysin and ubiquitin immunoreactivities of the gracile nucleus. Almost all spheroids showed strong immunostaining for (A–C) γ-syn and (E–G) β-syn in the gracile nucleus of gad mice from 3 to 32 weeks of age (A, 3 weeks; B and E, 12 weeks; C and F, 20 weeks; G, 32 weeks). Numerous γ-syn-positive spheroids (B, arrowheads) and occasional neurites (B, arrow) are demonstrated. Spheroids from wild-type mice at 20 weeks were also immunopositive for (D) γ-syn (arrowheads) and (H) β-syn (arrowhead). (I) Very little α-syn immunoreactivity was observed in *gad* mouse spheroids (12 weeks, arrowheads). (J) Also, as a positive control, there are any synaptic regions that could be indicated as being positive of α-syn in wild-type mouse (arrows) as well as in gad mouse (I, arrows), but α-syn was not detected in wild-type mouse spheroids (20 weeks, arrowheads). (K) Ubiquitin immunoreactivity in the *gad* mouse gracile nucleus (20 weeks) appeared in dots (arrows) but was not apparent in spheroids (arrowheads). (L) Ubiquitin-positive immunoreactivity was seen in both spheroids (arrowheads) and dots (arrows) in wild-type mice (20 weeks). For synaptophysin, except for the similar immunostaining pattern of synapses, the limited number of spheroids that were immunopositive exhibited diffuse or spotty staining (arrowheads) that was seen only in the center of spheroids at 20 weeks in both (M) *gad* and (0) wild-type mice. Indeed, *gad* mice had more synaptophysin immunoreactivity than did wild-type mice. (N) At 32 weeks, *gad* mice displayed a punctate distribution pattern of synaptophysin along synapses (arrowhead) or surrounding cell bodies, with a few densely stained spheroids (arrow). (P) In contrast, wild-type mice displayed an in situ expression pattern that was enriched in the spheroids at 32 weeks of age (arrowheads). Bar = 50 μm.

possible temporal relationships between spheroid formation and α-, β- and γ-synucleins in the *gad* mouse brain has not yet been proven. Because the *gad* mouse constitutes a neurodegenerative model for the study of spheroid proliferation in axonal termini, we therefore examined spheroid pathology using antibodies directed against α-, β- and γ-syn. Given that dystrophic swollen axons—the primary *gad* lesion observed in the gracile nucleus—result from spheroid proliferation, we quantitated spheroid formation and immunoreactivity in the medulla and upper cervical spinal cord regions over the lifetime of *gad* mice (Fig. 2F and Table 1).

We initially found that γ-syn-positive spheroids were more conspicuous than HE-stained spheroids during the early stage of age, suggesting that γ-syn is more sensitive and specific than HE for detecting spheroid formation in *gad* mice. β-syn was first detected in spheroids 8 weeks later than γ-syn. This result raises the possibility that the mechanism by which β-syn accumulates in spheroids differs from that of γ-syn and that γ-syn may play a more important role in the pathogenesis of the *gad* mutation. A recent study suggested that synucleins may help to regulate proteasome function by modulating 20S proteasome activity in the case

Table 1
Chronological change in the degree of immunoreactivity for spheroids stained for α-, β- and γ-synuclein and ubiquitin in the medulla and upper cervical cord of *gad* mice

	gad 3 weeks	*gad* 12 weeks	*gad* 20 weeks	*gad* 32 weeks	Wild-type 20 weeks	Wild-type 32 weeks
α-syn	−[a]	±	±	±	−	−
β-syn	−	+	++	+++	+	+
γ-syn	++	++	+++	+	+	+
ub-s[b]	−	−	−	−	+	+
ub-d[c]	−	++	+++	+	+	+

[a] Immunoreactivity: +++, strong; ++, moderate; + to ±, weaker to weak; −, not detectable.
[b] Ubiquitin immunoreactivity in the spheroids.
[c] Ubiquitin immunoreactivity in the dot-like structures.

of γ-syn and by affecting the 26S proteasome in the case of β-syn [34]. Thus, the fact that each of these two synucleins exhibits a distinct time course of spheroid accumulation may reflect differences in their metabolic regulation. Furthermore, γ-syn has a very different pattern of localization in neurons as compared with α-syn and β-syn [27].

Antibodies to ubiquitin recognize most spheroids, although it is unclear whether this recognition reflects sequestered free ubiquitin or ubiquitinated proteins [25,39]. Furthermore, the ubiquitinated substrates in spheroids have not been identified. We show here in *gad* mice that ubiquitin is absent from spheroids but is present in dot-like structures, which is consistent with a previous study [40]. Recently, we demonstrated that the loss of functional UCH-L1 leads to a decrease in free ubiquitin in *gad* mice [24]. In contrast, overexpression of UCH-L1 causes an increase in ubiquitin in both cultured cells and mice [24]. Therefore, we suggest that UCH-L1 ensures ubiquitin stability via prolonging the ubiquitin half-life within neurons as an important carrier protein, and loss of functional UCH-L1 may thus lead to inadequate ubiquitination via a decrease in free ubiquitin. Thus, the reduction in ubiquitin might be responsible for the absence of ubiquitin in *gad* mouse spheroids. Ubiquitin is, however, often detected in spheroid bodies during neurodegenerative diseases [2,41]. In addition, an increase in ubiquitin expression was reported in spheroid bodies in the brains of aged monkeys [31]. Despite the presence of ubiquitin in spheroid bodies in these systems, our data indicate that ubiquitination may not be required for the formation of spheroid bodies.

We found that spheroids were positive for both β- and γ-syn but were slight for α-syn in *gad* mice. Lewy bodies in PD and DLB brains are positive for both α-syn [36] and UCH-L1 [20], whereas we did not detect Lewy bodies or Lewy neurites in *gad* mouse brain. These observations suggest that the molecular mechanism of β- and γ-syn accumulation in *gad* spheroids is different from that in Lewy bodies. β-syn inhibits fibril accumulation of α-syn [11]. Thus, early accumulation of β-syn in the spheroids of *gad* mice may inhibit the accumulation of α-syn in spheroids or axon terminals. It remains unclear whether γ-syn has a similar effect on the accumulation of α-syn. Alternatively, fibril formation of α-syn might be affected by the existence of UCH-L1, and lack of UCH-L1 in the *gad* mouse might result in the suppression of α-syn aggregation in vivo. UCH-L1 was reported to have ubiquitin ligase activity that increased the amount of polyubiquitinated α-syn via K63-linked ubiquitination [19]. Other recent studies have shown that UCH-L1 can deubiquitinate polyubiquitinated α-syn with K48-linked ubiquitination [13,30]. Thus, a close relationship between UCH-L1 and α-syn has been implicated. Aggregates of β-syn and γ-syn have been found in dystrophic neurites associated with PD and other neurodegenerative diseases [7]. Neither protein, however, is detected in Lewy bodies in PD and DLB. Consequently, β-syn and γ-syn pathology may be more specific to spheroid disorders.

Pathological accumulations of β-syn and γ-syn were previously reported in neurological diseases [7]. β-syn is a presynaptic protein and *gad* degeneration starts at the presynapse of the gracile nuclei. Local accumulated β-syn may interfere with other presynaptic proteins in the degenerating terminals. We observed that a presynaptic protein, synaptophysin, was weakly detected in spheroids but strongly expressed in healthy synapses in *gad* mice. This result may support the idea of the effect of locally accumulated β-syn.

Overexpression of γ-syn may influence neurofilament network integrity [4]. Distinct from wild-type mice, in *gad* mice γ-syn immunoreactivity in the spheroids appeared in the gracile nucleus from an early stage, which might contribute to the dysfunction of the nervous system, possibly by interrupting axonal transport. Ubiquitin is known to be transported over long distances via slow axonal transport to synapses [3]. Ubiquitin reduction and the consequent inadequate ubiquitination of proteins may trigger accumulation of proteins that should undergo ubiquitin-dependent degradation. An age-dependent increase in γ- and β-syn-positive spheroids in *gad* mice resembles the accumulation of amyloid-β in spheroids of these mice [12]. Amyloid precursor protein has been shown to be transported by a fast axonal flow [16]. The abnormal accumulation of various proteins at terminals might affect axonal transport from the ganglia, leading to the dying-back type of degeneration of axons with formation of spheroid bodies. The mechanisms involved, however, will require more detailed studies of UCH-L1 and synucleins.

Acknowledgements

We thank Miss S. Kikuchi for assistance in preparation of the sections and Ms. M. Shikama for the care and breeding of animals. This work was supported in part by Grants-in-Aid for Scientific Research from the Ministry of Health, Labour and Welfare of Japan; Grants-in-Aid for Scientific Research from the Ministry of Education, Culture, Sports,

Science and Technology of Japan; a grant from the Organization for Pharmaceutical Safety and Research; and a grant from the Japan Science and Technology Agency.

References

[1] J. Aicardi, P. Castelein, Infantile neuroaxonal dystrophy, Brain 102 (1979) 727–748.
[2] N. Arai, Grumose or foamy spheroid bodies involving astrocytes in the human brain, Neuropathol. Appl. Neurobiol. 21 (1995) 238–245.
[3] A. Bizzi, B. Schaetzle, A. Patton, P. Gambetti, L. Autilio-Gambetti, Axonal transport of two major components of the ubiquitin system: free ubiquitin and ubiquitin carboxyl-terminal hydrolase PGP 9.5, Brain Res. 548 (1991) 292–299.
[4] V.L. Buchman, J. Adu, L.G. Pinon, N.N. Ninkina, A.M. Davies, Persyn, a member of the synuclein family, influences neurofilament network integrity, Nat. Neurosci. 1 (1998) 101–103.
[5] V.L. Buchman, H.J. Hunter, L.G. Pinon, J. Thompson, E.M. Privalova, N.N. Ninkina, A.M. Davies, Persyn, a member of the synuclein family, has a distinct pattern of expression in the developing nervous system, J. Neurosci. 18 (1998) 9335–9341.
[6] M. Farrer, J. Kachergus, L. Forno, S. Lincoln, D.S. Wang, M. Hulihan, D. Maraganore, K. Gwinn-Hardy, Z. Wszolek, D. Dickson, J.W. Langston, Comparison of kindreds with parkinsonism and alpha-synuclein genomic multiplications, Ann. Neurol. 55 (2004) 174–179.
[7] J.E. Galvin, K. Uryu, V.M. Lee, J.Q. Trojanowski, Axon pathology in Parkinson's disease and Lewy body dementia hippocampus contains alpha-, beta-, and gamma-synuclein, Proc. Natl. Acad. Sci. U. S. A. 96 (1999) 13450–13455.
[8] J.E. Galvin, B. Giasson, H.I. Hurtig, V.M. Lee, J.Q. Trojanowski, Neurodegeneration with brain iron accumulation, type 1 is characterized by alpha-, beta-, and gamma-synuclein neuropathology, Am. J. Pathol. 157 (2000) 361–368.
[9] M. Goedert, M.G. Spillantini, Dewy body diseases and multiple system atrophy as alpha-synucleinopathies, Mol. Psychiatry 3 (1998) 462–465.
[10] W. Halliday, The nosology of Hallervorden-spatz disease, J. Neurol. Sci. 134 (1995) 84–91 (Suppl.).
[11] M. Hashimoto, E. Rockenstein, M. Mante, M. Mallory, E. Masliah, beta-synuclein inhibits alpha-synuclein aggregation: a possible role as an anti-parkinsonian factor, Neuron 32 (2001) 213–223.
[12] N. Ichihara, J. Wu, D.H. Chui, K. Yamazaki, T. Wakabayashi, T. Kikuchi, Axonal degeneration promotes abnormal accumulation of amyloid beta-protein in ascending gracile tract of gracile axonal dystrophy (GAD) mouse, Brain Res. 695 (1995) 173–178.
[13] Y. Imai, M. Soda, R. Takahashi, Parkin suppresses unfolded protein stress-induced cell death through its E3 ubiquitin-protein ligase activity, J. Biol. Chem. 275 (2000) 35661–35664.
[14] T. Kikuchi, M. Mukoyama, K. Yamazaki, H. Moriya, Axonal degeneration of ascending sensory neurons in gracile axonal dystrophy mutant mouse, Acta Neuropathol. (Berl.) 80 (1990) 145–151.
[15] Y. Kon, D. Endoh, T. Iwanaga, Expression of protein gene product 9.5, a neuronal ubiquitin C-terminal hydrolase, and its developing change in sertoli cells of mouse testis, Mol. Reprod. Dev. 54 (1999) 333–341.
[16] E.H. Koo, S.S. Sisodia, D.-R. Archer, L.J. Martin, A. Weidemarm, K. Beyreuther, P. Fischer, C.L. Masters, D.L. Price, Precursor of amyloid protein in Alzheimer disease undergoes fast anterograde axonal transport, Proc. Natl. Acad. Sci. U. S. A. 87 (1990) 1561–1565.
[17] R. Kruger, W. Kuhn, T. Muller, D. Woitalla, M. Graeber, S. Kosel, H. Przuntek, J.T. Epplen, L. Schols, O. Riess, Ala30Pro mutation in the gene encoding alpha-synuclein in Parkinson's disease, Nat. Genet. 18 (1998) 106–108.
[18] C. Lavedan, E. Leroy, A. Dehejia, S. Buchholtz, A. Dutra, R.L. Nussbaum, M.H. Polymeropoulos, Identification, localization and characterization of the human gamma-synuclein gene, Hum. Genet. 103 (1998) 106–112.
[19] Y. Liu, L. Fallon, H.A. Lashuel, Z. Liu, P.T. Lansbury Jr., The UCH-L1 gene encodes two opposing enzymatic activities that affect alpha-synuclein degradation and Parkinson's disease susceptibility, Cell 111 (2002) 209–218.
[20] J. Lowe, H. McDermott, M. Landon, R.J. Mayer, K.D. Wilkinson, Ubiquitin carboxyl-terminal hydrolase (PGP 9.5) is selectively present in ubiquitinated inclusion bodies characteristic of human neurodegenerative diseases, J. Pathol. 161 (1990) 153–160.
[21] H. Miura, K. Oda, C. Endo, K. Yamazaki, H. Shibasaki, T. Kikuchi, Progressive degeneration of motor nerve terminals in GAD mutant mouse with hereditary sensory axonopathy, Neuropathol. Appl. Neurobiol. 19 (1993) 41–51.
[22] M. Mukoyama, K. Yamazaki, T. Kikuchi, T. Tomita, Neuropathology of gracile axonal dystrophy (GAD) mouse. An animal model of central distal axonopathy in primary sensory neurons, Acta Neuropathol. (Berl) 79 (1989) 294–299.
[23] K. Nishikawa, H. Li, R. Kawamura, H. Osaka, Y.L. Wang, Y. Hara, T. Hirokawa, Y. Manago, T. Amano, M. Noda, S. Aoki, K. Wada, Alterations of structure and hydrolase activity of parkinsonism-associated human ubiquitin carboxyl-terminal hydrolase L1 variants, Biochem. Biophys. Res. Commun. 304 (2003) 176–183.
[24] H. Osaka, Y.L. Wang, K. Takada, S. Takizawa, R. Setsuie, H. Li, Y. Sato, K. Nishikawa, Y.J. Sun, M. Sakurai, T. Harada, Y. Hara, I. Kimura, S. Chiba, K. Namikawa, H. Kiyama, M. Noda, S. Aoki, K. Wada, Ubiquitin carboxy-terminal hydrolase L1 binds to and stabilizes monoubiquitin in neuron, Hum. Mel. Genet. 12 (2003) 1945–1958.
[25] Y. Oya, H. Nakayasu, N. Fujita, K. Suzuki, Pathological study of mice with total deficiency of sphingolipid activator proteins (SAP knockout mice), Acta Neuropathol. (Berl.) 96 (1998) 29–40.
[26] M.H. Polymeropoulos, C. Lavedan, E. Leroy, S.E. Ide, A. Dehejia, A. Dutra, B. Pike, H. Root, J. Rubenstein, R. Boyer, E.S. Stenroos, S. Chandrasekharappa, A. Athanassiadou, T. Papapetropoulos, W.G. Johnson, A.M. Lazzarini, R.C. Duvoisin, G. Di Iorio, L.I. Golbe, R.L. Nussbaum, Mutation in the alpha-synuclein gene identified in families with Parkinson's disease, Science 276 (1997) 2045–2047.
[27] M.C. Quilty, W.P. Gai, D.L. Pountney, A.K. West, J.C. Vickers, Localization of alpha-, beta-, and gamma-synuclein during neuronal development and alterations associated with the neuronal response to axonal trauma, Exp. Neurol. 182 (2003) 195–207.
[28] K. Saigoh, Y.L. Wang, J.G. Suh, T. Yamanishi, Y. Sakai, H. Kiyosawa, T. Harada, N. Ichihara, S. Wakana, T. Kikuchi, K. Wada, Intragenic deletion in the gene encoding ubiquitin carboxy-terminal hydrolase in gad mice, Nat. Genet. 23 (1999) 47–51.
[29] K. Saito, T. Yokoyama, M. Okaniwa, S. Kamoshita, Neuropathology of chronic vitamin E deficiency in fatal familial intrahepatic cholestasis, Acta Neuropathol. (Berl) 58 (1982) 187–192.
[30] D.M. Sampathu, B.I. Giasson, A.C. Pawlyk, J.Q. Trojanowski, V.M. Lee, Ubiquitination of alpha-synuclein is not required for formation of pathological inclusions in alpha-synucleinopathies, Am. J. Pathol. 163 (2003) 91–100.
[31] C. Schultz, E.J. Dick, A.B. Cox, G.B. Hubbard, E. Braak, H. Braak, Expression of stress proteins alpha B-crystallin, ubiquitin, and hsp27 in pallido-nigral spheroids of aged rhesus monkeys, Neurobiol. Aging 22 (2001) 677–682.
[32] R. Sidman, J.B. Angevine, E.T. Pierce, Atlas of the Mouse Brain and Spinal Cord, Harvard Univ. Press, Cambridge, 1971.
[33] A.B. Singleton, M. Farrer, J. Johnson, A. Singleton, S. Hague, J. Kachergus, M. Hulihan, T. Peuralinna, A. Dutra, R. Nussbaum, S. Lincoln, A. Crawley, M. Hanson, D. Maraganore, C. Adler, M.R. Cookson, M. Muenter, M. Baptista, D. Miller, J. Blancato, J. Hardy, K. Gwinn-Hardy, Alpha-synuclein locus triplication causes Parkinson's disease, Science 302 (2003) 841.
[34] H.M. Synder, K. Mensah, I. Surgucheva, B. Festoff, A. Matouschek, A. Surguchov, B. Wolozin, Effect of alpha, beta and gamma synuclein

on the proteasomal pathways: 20S ubiquitin-independent, 26S ubiquitin-indenedent and 26S ubiquintin-dependent. Program No.132.8. Abstract viewer/Itinerary Planner. Society for Neuroscience, Washinton, DC, 2003.

[35] A. Takeda, M. Mallory, M. Sundsmo, W. Honer, L. Hansen, E. Masliah, Abnormal accumulation of NACP/alpha-synuclein in neurodegenerative disorders, Am. J. Pathol. 152 (1998) 367–372.

[36] A. Takeda, M. Hashimoto, M. Mallory, M. Sundsumo, L. Hansen, E. Masliah, C-terminal alpha-synuclein immunoreactivity in structures other than Lewy bodies in neurodegenerative disorders, Acta Neuropathol. (Berl.) 99 (2000) 296–304.

[37] P.H. Tu, J.E. Galvin, M. Baba, B. Giasson, T. Tomita, S. Leight, S. Nakajo, T. Iwatsubo, J.Q. Trojanowski, V.M. Lee, Glial cytoplasmic inclusions in white matter oligodendrocytes of multiple system atrophy brains contain insoluble alpha-synuclein, Ann. Neurol. 44 (1998) 415–422.

[38] K.D. Wilkinson, S. Deshpande, C.N. Larsen, Comparisons of neuronal (PGP 9.5) and non-neuronal ubiquitin C-terminal hydrolases, Biochem. Soc. Trans. 20 (1992) 631–637.

[39] D. Willwohl, M. Kettner, H. Braak, G.B. Hubbard, E.J. Dick Jr., A.B. Cox, C. Schultz, Pallido-nigral spheroids in nonhuman primates: accumulation of heat shock proteins in astroglial processes, Acta Neuropathol. (Berl) 103 (2002) 276–280.

[40] J. Wu, N. Ichihara, D.H. Chui, K. Yamazaki, T. Kikuchi, Abnormal ubiquitination of dystrophic axons in centralnervous system of gracile axonal dystrophy (gad) mutant mouse, Alzheimer's Res. 47 (1996) 163–168.

[41] T. Yamada, H. Akiyama, P.L. McGeer, Two types of spheroid bodies in the nigral neurons in Parkinson's disease, Can. J. Neurol. Sci. 18 (1991) 287–294.

[42] K. Yamazaki, N. Wakasugi, T. Tomita, T. Kikuchi, M. Mukoyama, K. Ando, Gracile axonal dystrophy (GAD), a new neurological mutant in the mouse, Proc. Soc. Exp. Biol. Med. 187 (1988) 209–215.

[43] K. Yamazaki, H. Moriya, T. Wakabayashi, T. Kikuchi, Substance β-like immunoreactivity in the gracile nucleus and fasciculus in old mice, Neurosci. Lett. 106 (1989) 258–260.

[44] K. Yamazaki, A. Kobayashi, A. Kumazawa, T. Wakabayashi, K. Takeki, Axonal degeneration in the central nervous system of gracile axonal dystroph (gad) mice progresses like in human spinocerebellar ataxias, Biomed. Res. 12 (1991) 143–148.

Brain-derived neurotrophic factor-dependent unmasking of "silent" synapses in the developing mouse barrel cortex

Chiaki Itami*, Fumitaka Kimura†‡, Tomoko Kohno*, Masato Matsuoka§, Masumi Ichikawa¶, Tadaharu Tsumoto†‡, and Shun Nakamura*‖

*Division of Biochemistry and Cellular Biology, National Institute of Neuroscience, Tokyo 187-8502, Japan; †Division of Neurophysiology, Osaka University Graduate School of Medicine, Osaka 565-0871, Japan; ‡Core Research for Evolutional Science and Technology, Japan Science and Technology Corporation, Kawaguchi 332-0012, Japan; §Division of Neurobiology and Anatomy, Department of Sensory and Integrative Medicine, Niigata University Graduate School of Medical and Dental Sciences, Niigata, Niigata 951-8510, Japan; and ¶Department of Developmental Morphology, Tokyo Metropolitan Institute for Neuroscience, Tokyo 183-8526, Japan

Edited by Hans Thoenen, Max Planck Institute of Neurobiology, Martinsried, Germany, and approved August 15, 2003 (received for review April 3, 2003)

Brain-derived neurotrophic factor (BDNF) is a critical modulator of central synaptic functions such as long-term potentiation in the hippocampal and visual cortex. Little is known, however, about its role in the development of excitatory glutamatergic synapses *in vivo*. We investigated the development of *N*-methyl-D-aspartate (NMDA) receptor (NMDAR)-only synapses (silent synapses) and found that silent synapses were prominent in acute thalamocortical brain slices from BDNF knockout mice even after the critical period. These synapses could be partially converted to α-amino-3-hydroxy-5-methyl-4-isoxazolepropionic acid receptor (AMPAR)-containing ones by adding back BDNF alone to the slice or fully converted to together with electric stimulation without affecting NMDAR transmission. Electric stimulation alone was ineffective under the BDNF knockout background. Postsynaptically applied TrkB kinase inhibitor or calcium-chelating reagent blocked this conversion. Furthermore, the AMPAR C-terminal peptides essential for interaction with PDZ proteins postsynaptically prevented the unmasking of silent synapses. These results suggest that endogenous BDNF and neuronal activity synergistically activate AMPAR trafficking into synaptic sites.

Neurotrophins had been identified as survival and neuronal differentiation factors in cell and tissue cultures (1) as well as regulatory factors for axonal and dendrite formation (2). Recently, they have been recognized as modulators for synaptic plasticity (3, 4). More direct evidence showed that locally applied brain-derived neurotrophic factor (BDNF) up-regulated postsynaptic Ca^{2+}-transients and synaptic potentiation at dendritic spines (5). However, the role of BDNF on the development of cortical excitatory and inhibitory synapses *in vivo* is uncertain. The existence of *N*-methyl-D-aspartate (NMDA) receptor (NMDAR)-only synapses (silent synapses) early in the critical period and the gradual conversion of these synapses to α-amino-3-hydroxy-5-methyl-4-isoxazolepropionic acid (AMPA) receptor (AMPAR)-containing ones have been reported and widely accepted as an important maturational step of glutamatergic synapses (6–8). Neuronal activity is supposed to regulate postsynaptic glutamate receptor trafficking, thus leading to the activation of AMPAR transmission (9). In the present study, we inquired about the role of endogenous BDNF on the development of "silent" synapses and provided evidence that BDNF is crucial for the maturation of AMPAR-mediated transmission in the developing mouse barrel cortex. We found that NMDAR-only synapses dominate in the initial phase of the critical period just after birth, and these synapses change to AMPAR-containing ones at the end of the critical period when examined in the acute thalamocortical brain slices under a whole-cell patch–clamp configuration. This change is mostly blocked in BDNF knockout mice but can be converted to be AMPAR-transmissible by adding back BDNF to the acute slices without affecting NMDAR transmission. Furthermore, the conversion required intact C-terminal amino acid residues of AMPAR subunits, suggesting that BDNF regulates one step of AMPAR trafficking into synaptic sites. Thus, our result showed another role of BDNF in the postsynaptic maturation of NMDAR-only synapses into AMPAR transmissible ones.

Materials and Methods

Animals. A line of BDNF-knockout mice generated in the C57BL/6 genetic background was bred in-house and genotyped (10). The experimental protocols were approved by the Ethics Review Committee for Animal Experimentation of the National Institute of Neuroscience. All experiments using the knockout mice phenotype were analyzed under double-blind conditions with no knowledge of genotype, which was analyzed by someone who had not been informed about the result of phenotype analysis.

Electron Microscopy. Specimens were obtained from four mice at postnatal day (P)8. To avoid developmental heterogeneity among cortical barrels, we chose a particular barrel (C2) and layer four neurons in the C2 hollow region and prepared thin sections (1 μm) from the C2 region. Statistical analysis was performed by using the Mann–Whitney *U* test, and the data were assumed as significant when $P < 0.05$. More detailed information is in *Supporting Methods*, which is published as supporting information on the PNAS web site, www.pnas.org.

Preparation of Slices, Electrophysiology, and Data Analysis. Thalamocortical slices (400–500 μm thick) were prepared from neonatal mice (2–14 days old; the day of birth was defined as P0) by using a rotor slicer, and electrophysiological recording was carried out as described (11). More detailed information is provided in *Supporting Methods*.

Results

Subtle Difference of Synaptic Structure but No Difference of Synaptic Density Among BDNF Genotypes. BDNF regulates both axonal and dendritic morphology (12), thus it could establish neuronal connectivity and synaptic efficacy. In our previous observation during a critical period (10), BDNF and its receptor TrkB were transiently expressed in a barrel-hollow region where thalamic afferents make strong excitatory synapses on cortical neurons (13). BDNF knockout mice, however, did not show any anatomical abnormality examined by cytochrome oxidase and Nissl staining or fluorescent

This paper was submitted directly (Track II) to the PNAS office.

Abbreviations: BDNF, brain-derived neurotrophic factor; NMDA, *N*-methyl-D-aspartate; NMDAR, NMDA receptor; AMPA, α-amino-3-hydroxy-5-methyl-4-isoxazolepropionic acid; AMPAR, AMPA receptor; P*n*, postnatal day *n*.

‖To whom correspondence should be addressed. E-mail: nakamura@ncnp.go.jp.